Eur. J. Stat. 6 (2026) 7
doi: 10.28924/ada/stat.6.7

Modeling Maternal Blood Loss Using the Exponentiated Kumaraswamy–Inverse Lomax Distribution: Applications to Diverse Real-Life Data

Benson Ade Eniola Afere[1,*], Deborah Aladi Daikwo[1], Ekele Vincent Aguda[2], Yahaya Baba Usman[3], Sule Omeiza Bashiru[4], Bolarinwa Bolaji[1]

[1] *Department of Mathematical Sciences, Prince Abubakar Audu University, Anyigba, Nigeria*
baafere@gmail.com, daikwo.da@ksu.edu.ng, bolarinwa.s.bolaji@gmail.com
[2] *Department of Mathematics, Nigeria Maritime University, Okerenkoko, Nigeria*
vincentekele@yahoo.com
[3] *Department of Mathematics and Statistics, Federal Polytechnic, Idah, Kogi State, Nigeria*
ybusman_2005@yahoo.com
[4] *Department of Mathematics and Statistics, Confluence University of Science and Technology, Osara, Kogi State, Nigeria*
bash0140@gmail.com
[*] *Correspondence: baafere@gmail.com*

Abstract. This study introduces the Exponentiated Kumaraswamy–Inverse Lomax (EK–IL) distribution as a flexible and robust statistical model for analyzing maternal blood loss during delivery. The proposed distribution effectively accommodates skewness and heavy-tailed behavior, which are common characteristics of clinical data. Model parameters are estimated using the maximum likelihood method, and the performance of the EK–IL distribution is evaluated through goodness-of-fit measures and information criteria. Comparative analyses demonstrate that the proposed model outperforms several well-known competing distributions. Further validation using four additional real datasets confirms the adaptability and robustness of the EK–IL distribution. The results suggest that the EK–IL model provides a powerful framework for medical data analysis and broader applications in applied statistics.

1. Introduction

Data science is the process of transforming raw information into actionable knowledge. It integrates techniques from statistics, scientific research, artificial intelligence, and computer-based data analysis [1]. These methods support the collection, cleaning, preparation, and analysis of data in order to identify patterns and trends. In statistics, a central objective is the identification of an appropriate mathematical model, typically a probability distribution, capable of describing the behavior of observed data. Once a suitable distribution is established, important statistical

Received: 17 Jan 2026.
Key words and phrases. Kumaraswamy distribution; inverse Lomax distribution; maternal blood loss; maximum likelihood estimation; goodness-of-fit tests; Monte Carlo simulation.

characteristics such as the mean, variability, skewness, and tail behavior can be derived. These measures provide essential information for prediction, decision-making, and further scientific analysis.

Selecting an appropriate probability distribution is often challenging. Classical distributions, such as the normal distribution, may fail to adequately describe real-world datasets, especially when the data exhibit asymmetry, heavy tails, or unusual shapes. To address these limitations, researchers have developed flexible families of probability distributions capable of capturing a wide range of behaviors [2, 3, 15, 18, 24]. These generalized models are particularly useful when extreme observations play an important role in the analysis.

In recent decades, considerable research has focused on developing flexible lifetime distributions through transformation and generalization techniques. These approaches often utilize generator functions or combine existing distributions to introduce additional parameters that enhance modeling flexibility and improve the ability to capture diverse data characteristics. One of the most influential developments in this area is the class of beta-generated distributions introduced by [2], which extends baseline distributions by allowing them to exhibit a wide variety of shapes and tail behaviors. In a similar vein, the Kumaraswamy distribution has attracted significant attention as a generator because of its closed-form cumulative distribution function, which offers substantial analytical convenience and facilitates tractable statistical inference [31].

Building on these developments, [32] proposed the Hybrid–Epanechnikov Transformed Kumaraswamy Distribution (HTKD), a flexible two-parameter model that integrates the Epanechnikov kernel within the Kumaraswamy framework. The study investigated the statistical properties of the proposed distribution and employed maximum likelihood estimation for parameter inference. Using COVID-19 mortality and survival datasets from Spain, Canada, and the United Kingdom, the results demonstrated that the HTKD model provided improved goodness-of-fit performance compared with several classical competing models according to the Akaike Information Criterion (AIC) and the Bayesian Information Criterion (BIC).

Another important distribution in reliability and survival analysis is the Inverse Lomax distribution, which represents the reciprocal form of the Lomax distribution [28, 29]. This distribution has been widely applied in reliability engineering, actuarial science, financial risk modeling, and survival studies due to its heavy-tailed characteristics and its ability to model decreasing hazard rates. Nevertheless, despite its usefulness, the standard Inverse Lomax distribution may exhibit limitations when modeling more complex data structures, particularly those involving non-monotonic hazard functions or unusual tail behaviors.

To improve flexibility, generator mechanisms based on the Kumaraswamy distribution [30] and exponentiation techniques have been proposed to extend baseline models. These developments have led to the Exponentiated Kumaraswamy-G family of distributions [31], where the notation "G" represents a baseline distribution. Motivated by this framework, the present study introduces the Exponentiated Kumaraswamy–Inverse Lomax (EK–IL) distribution, which combines

the heavy-tail characteristics of the Inverse Lomax distribution with the additional shape flexibility provided by the Kumaraswamy transformation and exponentiation. The resulting model is capable of capturing asymmetry, kurtosis variations, and complex hazard rate behaviors.

Many biomedical datasets exhibit features that require such flexible modeling approaches. For example, maternal blood loss during childbirth is a non-negative variable that typically displays strong right-skewness and may contain extreme values resulting from severe hemorrhage. Classical distributions such as the normal distribution are unsuitable for such data, and even commonly used positive-valued models like the gamma, lognormal, or Weibull distributions may fail to adequately capture both the central tendency and the extreme tail behavior.

Postpartum hemorrhage (PPH) is a major obstetric complication defined as blood loss of at least 500 mL after vaginal delivery or 1,000 mL after cesarean section [4]. Globally, PPH remains the leading direct cause of maternal mortality, accounting for approximately 70,000 deaths annually, with the majority occurring in low- and middle-income countries [5]. In Nigeria, the lifetime risk of maternal death is estimated to be approximately 1 in 22 [6], and maternal mortality rates remain among the highest worldwide [7]. Consequently, PPH represents a critical public health concern.

Accurate measurement of blood loss is essential for timely medical intervention. However, visual estimation, which is still widely practiced in many healthcare facilities, often underestimates large volumes and overestimates smaller amounts of blood loss. This practice introduces considerable measurement variability and observer bias [8,9]. These challenges further highlight the need for statistical models capable of accurately describing the distribution of blood loss data.

The proposed EK–IL distribution addresses this challenge by combining the heavy-tail behavior of the Inverse Lomax distribution [11] with the flexibility provided by the Kumaraswamy transformation and exponentiation [24]. This combination allows the model to effectively capture skewness, tail heaviness, and kurtosis, making it particularly suitable for modeling maternal blood loss data.

In this study, the EK–IL distribution is applied to analyze blood loss during and after childbirth in a Nigerian tertiary hospital. The objectives of the study are to examine the distributional characteristics of the data, estimate the parameters of the EK–IL model, compute summary measures such as means, variances, quantiles, and tail probabilities, and compare the EK–IL distribution with competing models using goodness-of-fit criteria that emphasize both overall fit and tail behavior. The results are interpreted in clinical terms, including the probability of blood loss exceeding clinically significant thresholds such as 500 mL and 1,000 mL. By integrating advanced statistical modeling with clinical interpretation, this study aims to provide improved insights into maternal blood loss patterns and support better planning and response strategies for postpartum hemorrhage management.

The remainder of this paper is structured as follows. Section 2 introduces the proposed distribution, while Section 3 details its statistical properties. Parameter estimation methods are presented in Section 4, and the real data application is discussed in Section 5. Finally, Section 6 concludes the paper with a summary of the findings and concluding remarks.

2. Creation of the Proposed EK–IL Distribution

Let X be a random variable following the Inverse Lomax distribution [11, 29]. Its cumulative distribution function (CDF) and probability density function (PDF) are respectively given by

$$F_{IL}(y;\lambda,\beta) = \left(1+\frac{\beta}{y}\right)^{-\lambda}, \qquad y>0,\ \lambda>0,\ \beta>0, \tag{1}$$

and

$$f_{IL}(y;\lambda,\beta) = \frac{\lambda\,\beta^{\lambda}\,y^{\lambda-1}}{(y+\beta)^{\lambda+1}}, \qquad y>0. \tag{2}$$

Similarly, consider T to be a random variable following the Kumaraswamy distribution [30], with CDF and PDF defined by

$$F_K(t;a,b) = 1-(1-t^a)^b, \qquad 0<t<1,\ a>0,\ b>0, \tag{3}$$

and

$$f_K(t;a,b) = ab\,t^{a-1}\,(1-t^a)^{b-1}, \qquad 0<t<1. \tag{4}$$

By introducing an additional exponentiation parameter $c>0$ to the Kumaraswamy distribution and adopting the Inverse Lomax distribution as the baseline, we define a new class of distributions. This class transforms the baseline random variable through $[F_K(F_{IL}(x;\lambda,\beta);a,b)]^c$, and is referred to as the *Exponentiated Kumaraswamy–Inverse Lomax* (EK–IL) distribution. The CDF of the EK–IL distribution is then given by

$$F(x;a,b,c,\beta,\lambda) = \left[1-\left(1-\left(1+\frac{\beta}{x}\right)^{-a\lambda}\right)^b\right]^c \mathbf{1}_{\{x>0\}}, \tag{5}$$

where $a,b,c>0$ are shape parameters, $\beta>0$ is a scale parameter, and $\lambda>0$ is the tail index parameter.

Differentiating Eq. (5) with respect to x yields the PDF of the EK–IL distribution:

$$\begin{aligned} f(x;a,b,c,\beta,\lambda) = {} & \frac{abc\,\lambda\beta}{x^2}\left(1+\frac{\beta}{x}\right)^{-a\lambda}\left[1-\left(1+\frac{\beta}{x}\right)^{-a\lambda}\right]^{b-1} \\ & \times\left\{1-\left[1-\left(1+\frac{\beta}{x}\right)^{-a\lambda}\right]^b\right\}^{c-1}\mathbf{1}_{\{x>0\}}. \end{aligned} \tag{6}$$

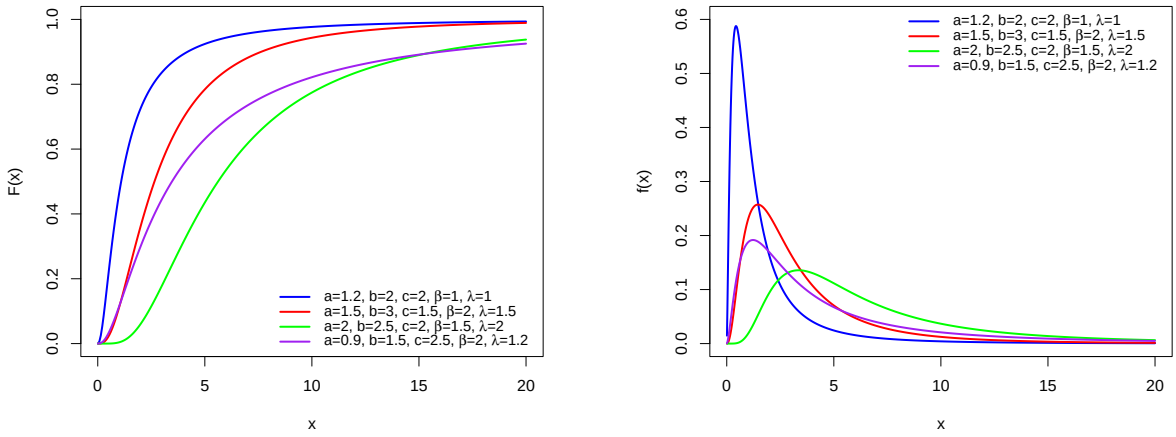

FIGURE 1. CDF and PDF of the EK–IL distribution for four combinations of parameters.

Using Eq. (5), the survival function can be expressed as:

$$S(x) = 1 - F(x) = 1 - \left[1 - \left(1 - \left(1 + \frac{\beta}{x}\right)^{-a\lambda}\right)^{b}\right]^{c} \mathbf{1}_{\{x>0\}}. \tag{7}$$

Combining Eqs. (6) and (7) gives the hazard rate function:

$$h(x) = \frac{abc\,\lambda\beta}{x^2}\left(1 + \frac{\beta}{x}\right)^{-a\lambda} \frac{\left[1 - \left(1 + \frac{\beta}{x}\right)^{-a\lambda}\right]^{b-1}}{\left\{1 - \left[1 - \left(1 + \frac{\beta}{x}\right)^{-a\lambda}\right]^{b}\right\}} \mathbf{1}_{\{x>0\}}. \tag{8}$$

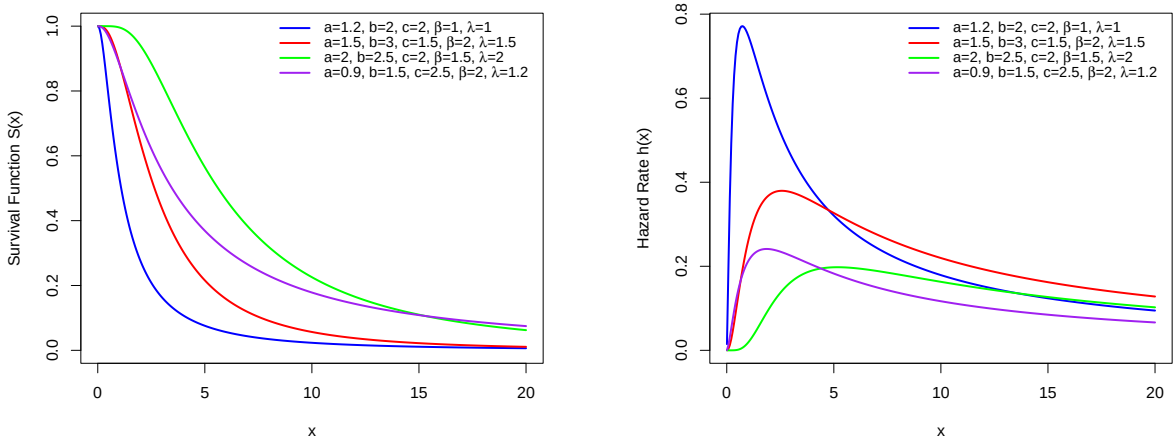

FIGURE 2. Survival and Hazard functions of the EK–IL distribution for four combinations of parameters.

From Eq. (7), the cumulative hazard function is:

$$H(x) = -\ln S(x) = -c \ln \left[1 - \left(1 - \left(1 + \frac{\beta}{x} \right)^{-a\lambda} \right)^{b} \right] \mathbf{1}_{\{x>0\}}. \tag{9}$$

Similarly, combining Eqs. (5) and (6) yields the reversed hazard rate function:

$$r(x) = \frac{abc\,\lambda\beta}{x^2} \left(1 + \frac{\beta}{x} \right)^{-a\lambda} \left[1 - \left(1 + \frac{\beta}{x} \right)^{-a\lambda} \right]^{b-1} \left\{ 1 - \left[1 - \left(1 + \frac{\beta}{x} \right)^{-a\lambda} \right]^{b} \right\}^{-1} \mathbf{1}_{\{x>0\}}. \tag{10}$$

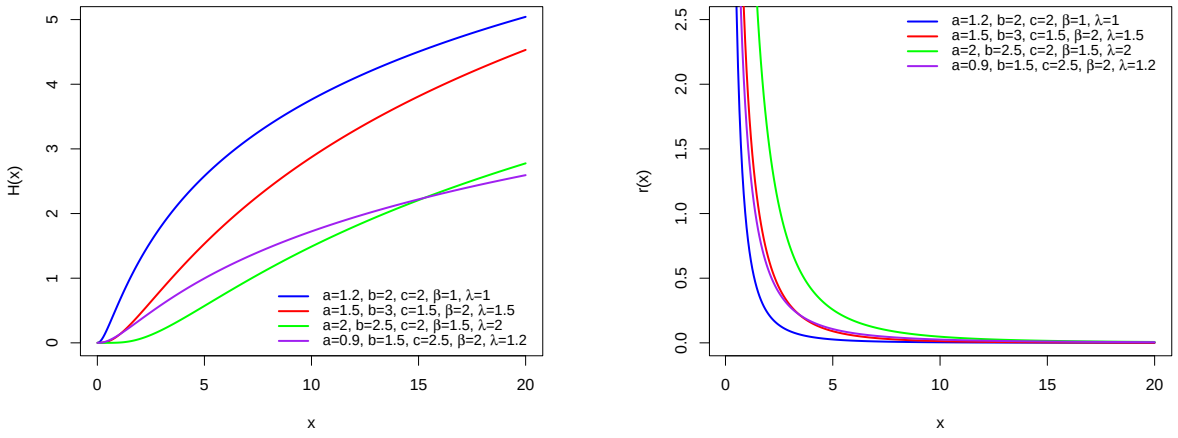

FIGURE 3. Cumulative hazard and Reversed hazard rate functions of the EK–IL distribution for four combinations of parameters.

The quantile function $Q(p)$, obtained by inverting Eq. (5), is:

$$Q(p) = \frac{\beta}{\left[1 - \left(1 - p^{1/c} \right)^{1/b} \right]^{-1/(a\lambda)} - 1}, \quad 0 < p < 1. \tag{11}$$

$Q(p)$ enables direct computation of percentiles and medians and is useful for simulating EK–IL random samples via the inverse transform method: generate $U \sim \text{Uniform}(0, 1)$, then compute $Q(U)$.

The graphical representations in Figures 1, 2, and 3 collectively illustrate the flexibility and diverse behavior of the EK–IL distribution under different parameter configurations. Figure 1 combines the CDF and PDF plots, showing how cumulative probability and density respond to variations in x. The CDF curves demonstrate that steeper slopes correspond to rapid accumulation of probability mass, while flatter shapes indicate heavier-tailed behavior. This flexibility allows the distribution to capture both early- and late-occurring events depending on parameter choices. The PDFs, on the other hand, reveal a variety of possible shapes, including unimodal, skewed, and heavy-tailed forms, confirming the adaptability of the EK–IL distribution to a wide range of empirical data scenarios.

In Figure 2, the survival and hazard functions are displayed side by side. The survival function illustrates the probability of surviving beyond a given threshold, with slower decay patterns indicating heavier tails and extended lifetimes, a key aspect in reliability and risk modeling. The hazard function plots reveal the distribution's ability to accommodate different failure rate behaviors, such as monotonically increasing, monotonically decreasing, bathtub-shaped, and unimodal hazard rates, each relevant for different real-world failure and deterioration processes.

Finally, Figure 3 presents the cumulative hazard and reversed hazard rate functions. The cumulative hazard function captures the accumulation of risk over time, providing insight into long-term failure patterns and allowing for direct comparisons of risk intensities across parameter settings. The reversed hazard rate function, by contrast, focuses on the instantaneous failure rate from the left side (early in the life cycle), highlighting scenarios where early-life failures are either more or less likely. Together, these paired plots offer a comprehensive visual understanding of how the EK–IL distribution can be tuned to model a diverse spectrum of lifetime behaviors.

3. Statistical Properties

3.1. **Quantile function.** Suppose X is a random variable following the EK–IL distribution with parameters $a, b, c, \beta, \lambda > 0$, and let U be a Uniform$(0, 1)$ random variable. Then the quantile function of X is given by

$$X = \frac{\beta}{\left[1 - \left(1 - U^{1/c}\right)^{1/b}\right]^{-1/(a\lambda)} - 1}, \quad 0 < U < 1. \tag{12}$$

The median is obtained by setting $u = 0.5$ in (12) and is given by

$$m = \frac{\beta}{\left[1 - \left(1 - 0.5^{1/c}\right)^{1/b}\right]^{-1/(a\lambda)} - 1}.$$

3.2. **Moments.** Moments provide useful information about the shape of the distribution, including measures such as mean (μ_1'), variance, skewness, and kurtosis. For the proposed model, the moment is given by

$$\mu_r' = \beta^r \, abc\lambda \sum_{k=0}^{\infty} (-1)^k \binom{c-1}{k} \frac{\Gamma(\alpha)\,\Gamma(r + b(1+k))}{\Gamma(\alpha + r + b(1+k))}. \tag{13}$$

The first four moments can be obtained by substituting $r = 1, 2, 3, 4$ into Eq. (13)

The mean (μ), variance (σ^2), skewness (S), and kurtosis (K) of the EK–IL distribution are given respectively as:

$$\mu = \mu_1',$$
$$\sigma^2 = \mu_2' - (\mu_1')^2,$$
$$S = \frac{\mu_3' - 3\mu_2'\mu_1' + 2(\mu_1')^3}{\sigma^3},$$
$$K = \frac{\mu_4' - 4\mu_3'\mu_1' + 6\mu_2'(\mu_1')^2 - 3(\mu_1')^4}{\sigma^4}.$$

.

[25] proposed a quantile-based approach for evaluating skewness, while [26] developed a corresponding measure for kurtosis. Bowley's skewness and Moors' kurtosis can be computed using

$$S_B = \frac{Q_{6/8} - 2Q_{4/8} + Q_{2/8}}{Q_{6/8} - Q_{2/8}}, \quad K_M = \frac{(Q_{7/8} - Q_{5/8}) + (Q_{3/8} - Q_{1/8})}{Q_{6/8} - Q_{2/8}},$$

where Q_p denotes the p-th quantile. Since the quantile function of the EK–IL distribution is available in a closed analytic form, these expressions can be directly employed to compute its skewness and kurtosis.

Table 1 presents descriptive statistics of the EK–IL distribution, summarizing central tendency, dispersion, skewness, and kurtosis.

TABLE 1. Summary of Descriptive Statistics for the EK–IL Distribution

Set	a	b	c	β	λ	Mean	Median	SD	Q1	Q3	IQR	S_B	K_M
1	2.0	3.0	1.5	1.0	0.5	0.6674	0.3913	1.0844	0.1825	0.7871	0.6046	0.3092	1.4981
2	1.5	2.0	2.0	0.8	1.2	2.6504	1.4776	8.6481	0.8158	2.7862	1.9704	0.3282	1.5869
3	3.0	1.5	1.0	2.0	0.7	8.7949	3.2895	45.4160	1.5354	7.2761	5.7407	0.3889	1.7650
4	2.5	2.5	1.2	1.5	1.0	3.5981	2.2536	5.2980	1.2461	4.1306	2.8845	0.3014	1.5180
5	4.0	3.0	2.0	0.5	0.9	1.9281	1.4151	1.9770	0.9090	2.2703	1.3613	0.2565	1.4522
6	1.2	2.8	1.8	2.2	1.5	3.9169	2.6349	5.0174	1.5220	4.5930	3.0710	0.2752	1.4812

Three-dimensional plots of Bowley's skewness and Moors' kurtosis for selected parameter values of the EK–IL distribution are presented in Figure 4.

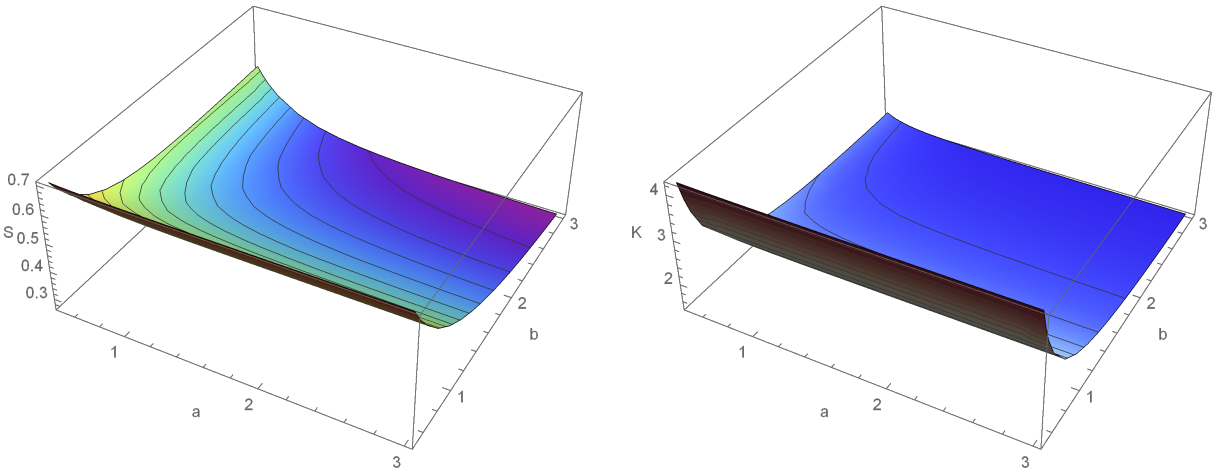

FIGURE 4. Bowley's skewness and Moors' kurtosis for the EK–IL distribution ($c = 1.5; \beta = 1.0; \lambda = 0.8$).

The descriptive statistics in Table 1 demonstrate the flexibility of the EK–IL distribution across parameter settings. Means vary from 0.67 (Set 1) to 8.79 (Set 3), showing its ability to capture both light- and heavy-tailed data. Medians are consistently below means, indicating positive skewness, which is confirmed by Bowley's skewness (0.26–0.39). Dispersion also varies widely: Set 3 shows the largest spread (SD $\approx$ 45.42; IQR $\approx$ 5.74), while Set 1 is more concentrated (SD $\approx$ 1.08; IQR $\approx$ 0.60). Moors' kurtosis (1.45–1.77) suggests moderate leptokurtosis, reflecting heavier-than-normal tails. Figure 4 further illustrates that skewness remains positive and kurtosis consistently exceeds 1, confirming the EK–IL distribution's adaptability in modeling skewed biomedical datasets such as maternal blood loss.

3.3. **Entropy Measures.** The Shannon entropy of a random variable X measures the average uncertainty in its possible outcomes, quantifying the expected information gained when observing X [27]. The Shannon entropy is generally defined as $H = -\int_0^\infty f(x)\log f(x)\,dx$.
For the proposed model, the Shannon entropy is given by

$$\begin{aligned} H = & -\log(abc\lambda\beta) + abc\lambda \sum_{m=0}^{\infty}\sum_{n=1}^{\infty} C_{m,n}\, Q(\alpha, n) \\ & - b(b-1)c \sum_{m=0}^{\infty}\sum_{n=1}^{\infty} C_{m,n}\, D(\alpha, n) - (c-1)\frac{abc\lambda}{\alpha} \sum_{m=0}^{\infty}\sum_{n=1}^{\infty}\sum_{r=1}^{\infty}\sum_{s=0}^{\infty} R_{m,n,r,s}\,. \end{aligned}$$

4. Parameter Estimation

Parameter estimation is a crucial step in statistical modeling, providing numerical values for the unknown parameters of a probability distribution based on observed data. For the EK–IL distribution, we employ the Maximum Likelihood Estimation (MLE) method, which is widely used due to its desirable asymptotic properties such as consistency, efficiency, and asymptotic normality.

4.1. **Maximum Likelihood Estimation.** Let $X_1, X_2, \ldots, X_n$ be a random sample of size n from the EK–IL distribution with probability density function defined earlier. The parameter vector is given by

$$\boldsymbol{\theta} = (a, b, c, \beta, \lambda).$$

The likelihood function for $\boldsymbol{\theta}$ is

$$L(\boldsymbol{\theta}) = \prod_{i=1}^{n} f(x_i; a, b, c, \beta, \lambda),$$

and the log-likelihood function is

$$\ell(\boldsymbol{\theta}) = \sum_{i=1}^{n} \ln f(x_i; a, b, c, \beta, \lambda).$$

To obtain the maximum likelihood estimators (MLEs), we differentiate the log-likelihood with respect to each parameter and set the derivatives equal to zero. For convenience, define the intermediate variables

$$z_i = \left(1 + \frac{\beta}{x_i}\right)^{-a\lambda}, \quad u_i = 1 - z_i, \quad v_i = 1 - u_i^b.$$

The score function is the gradient of the log-likelihood with respect to the parameters:

$$U(\boldsymbol{\theta}) = \left(\frac{\partial \ell}{\partial a}, \frac{\partial \ell}{\partial b}, \frac{\partial \ell}{\partial c}, \frac{\partial \ell}{\partial \lambda}, \frac{\partial \ell}{\partial \beta}\right)^T.$$

where the partial derivatives of $\ell(\theta)$ with respect to the parameters a, b, c, λ, and β are denoted by $\frac{\partial \ell}{\partial a}, \frac{\partial \ell}{\partial b}, \frac{\partial \ell}{\partial c}, \frac{\partial \ell}{\partial \lambda}, \frac{\partial \ell}{\partial \beta}$, and are explicitly given as follows:

$$\frac{\partial \ell}{\partial a} = \frac{n}{a} - \lambda \sum_{i=1}^{n} \ln\left(1 + \frac{\beta}{x_i}\right) + (b-1) \sum_{i=1}^{n} \frac{z_i \ln(1 + \beta/x_i)}{u_i} + (c-1) \sum_{i=1}^{n} \frac{b z_i u_i^{b-1} \ln(1 + \beta/x_i)}{v_i}.$$

$$\frac{\partial \ell}{\partial b} = \frac{n}{b} + \sum_{i=1}^{n} \ln u_i - (c-1) \sum_{i=1}^{n} \frac{u_i^b \ln u_i}{v_i}.$$

$$\frac{\partial \ell}{\partial c} = \frac{n}{c} + \sum_{i=1}^{n} \ln v_i.$$

$$\frac{\partial \ell}{\partial \lambda} = \frac{n}{\lambda} - (a-1) \sum_{i=1}^{n} \ln\left(1 + \frac{\beta}{x_i}\right) - \sum_{i=1}^{n} \ln\left(1 + \frac{\beta}{x_i}\right)$$

$$+ (b-1) \sum_{i=1}^{n} \frac{a z_i \ln(1 + \beta/x_i)}{u_i} + (c-1) \sum_{i=1}^{n} \frac{ab z_i u_i^{b-1} \ln(1 + \beta/x_i)}{v_i}.$$

$$\frac{\partial \ell}{\partial \beta} = \frac{n}{\beta} - (\lambda + 1 + \lambda(a-1)) \sum_{i=1}^{n} \frac{1}{x_i + \beta} + (b-1) \sum_{i=1}^{n} \frac{a\lambda z_i}{(x_i + \beta) u_i} + (c-1) \sum_{i=1}^{n} \frac{ab\lambda z_i u_i^{b-1}}{(x_i + \beta) v_i}.$$

In a nutshell, the score function of the EK–IL distribution provides a system of nonlinear equations in terms of the parameters a, b, c, λ, and β. Since these equations do not admit closed-form solutions, the MLEs must be obtained numerically. This formulation establishes the basis for parameter estimation and subsequent inference, highlighting the flexibility and tractability of the EK–IL distribution within likelihood-based methods.

4.2. **Fisher Information Matrix (FIM).** The observed Fisher information matrix for the EK–IL distribution is obtained by evaluating the negative Hessian of the log-likelihood function at the maximum likelihood estimates (MLEs), that is

$$\hat{\mathcal{I}}(\hat{\boldsymbol{\theta}}) = - \left. \frac{\partial^2 \ell(\boldsymbol{\theta})}{\partial \boldsymbol{\theta}\, \partial \boldsymbol{\theta}^T} \right|_{\boldsymbol{\theta} = \hat{\boldsymbol{\theta}}}.$$

Since the Hessian is symmetric, the observed information matrix inherits this symmetry. For the parameter vector $\boldsymbol{\theta} = (a, b, c, \beta, \lambda)^T$, the observed Fisher information takes the symmetric

5×5 form

$$\hat{\mathcal{I}}(\hat{\boldsymbol{\theta}}) = -\begin{bmatrix} \frac{\partial^2 \ell}{\partial a^2} & \frac{\partial^2 \ell}{\partial a \partial b} & \frac{\partial^2 \ell}{\partial a \partial c} & \frac{\partial^2 \ell}{\partial a \partial \beta} & \frac{\partial^2 \ell}{\partial a \partial \lambda} \\ \frac{\partial^2 \ell}{\partial b \partial a} & \frac{\partial^2 \ell}{\partial b^2} & \frac{\partial^2 \ell}{\partial b \partial c} & \frac{\partial^2 \ell}{\partial b \partial \beta} & \frac{\partial^2 \ell}{\partial b \partial \lambda} \\ \frac{\partial^2 \ell}{\partial c \partial a} & \frac{\partial^2 \ell}{\partial c \partial b} & \frac{\partial^2 \ell}{\partial c^2} & \frac{\partial^2 \ell}{\partial c \partial \beta} & \frac{\partial^2 \ell}{\partial c \partial \lambda} \\ \frac{\partial^2 \ell}{\partial \beta \partial a} & \frac{\partial^2 \ell}{\partial \beta \partial b} & \frac{\partial^2 \ell}{\partial \beta \partial c} & \frac{\partial^2 \ell}{\partial \beta^2} & \frac{\partial^2 \ell}{\partial \beta \partial \lambda} \\ \frac{\partial^2 \ell}{\partial \lambda \partial a} & \frac{\partial^2 \ell}{\partial \lambda \partial b} & \frac{\partial^2 \ell}{\partial \lambda \partial c} & \frac{\partial^2 \ell}{\partial \lambda \partial \beta} & \frac{\partial^2 \ell}{\partial \lambda^2} \end{bmatrix}.$$

The diagonal elements of this matrix correspond to the second derivatives with respect to each parameter and are given by

$$\begin{aligned} \frac{\partial^2 \ell}{\partial a^2} &= -\frac{n}{a^2}, \\ \frac{\partial^2 \ell}{\partial b^2} &= -\frac{n}{b^2}, \\ \frac{\partial^2 \ell}{\partial c^2} &= -\frac{n}{c^2}, \\ \frac{\partial^2 \ell}{\partial \beta^2} &= -\frac{n}{\beta^2} + (\lambda a + 1) \sum_{i=1}^{n} \frac{1}{(x_i + \beta)^2}, \\ \frac{\partial^2 \ell}{\partial \lambda^2} &= -\frac{n}{\lambda^2}. \end{aligned}$$

The off-diagonal elements represent the mixed second derivatives and are given by:

$$\begin{aligned} \frac{\partial^2 \ell}{\partial a \partial b} &= \sum_{i=1}^{n} \frac{z_i^a \log z_i \cdot \log \nu_i}{1 - z_i^a}, \\ \frac{\partial^2 \ell}{\partial a \partial c} &= 0, \\ \frac{\partial^2 \ell}{\partial a \partial \beta} &= \lambda \sum_{i=1}^{n} \frac{\log z_i}{x_i(1 + \beta / x_i)}, \\ \frac{\partial^2 \ell}{\partial a \partial \lambda} &= -\sum_{i=1}^{n} \log\left(1 + \frac{\beta}{x_i}\right), \\ \frac{\partial^2 \ell}{\partial b \partial c} &= \sum_{i=1}^{n} \frac{\nu_i^b \log \nu_i \cdot \log w_i}{1 - \nu_i^b}, \\ \frac{\partial^2 \ell}{\partial b \partial \beta} &= \sum_{i=1}^{n} \frac{a \lambda z_i^a \log z_i}{(1 - z_i^a)\nu_i} \cdot \frac{1}{x_i(1 + \beta / x_i)}, \\ \frac{\partial^2 \ell}{\partial b \partial \lambda} &= \sum_{i=1}^{n} \frac{a z_i^a \log z_i \cdot \log \nu_i}{(1 - z_i^a)\nu_i} \cdot \log\left(1 + \frac{\beta}{x_i}\right), \\ \frac{\partial^2 \ell}{\partial c \partial \beta} &= \sum_{i=1}^{n} \frac{b \nu_i^b \log \nu_i}{(1 - \nu_i^b) w_i} \cdot \frac{a \lambda z_i^a \log z_i}{(1 - z_i^a)\nu_i} \cdot \frac{1}{x_i(1 + \beta / x_i)}, \\ \frac{\partial^2 \ell}{\partial c \partial \lambda} &= \sum_{i=1}^{n} \frac{b \nu_i^b \log \nu_i}{(1 - \nu_i^b) w_i} \cdot \frac{a z_i^a \log z_i}{(1 - z_i^a)\nu_i} \cdot \log\left(1 + \frac{\beta}{x_i}\right), \end{aligned}$$

$$\frac{\partial^2 \ell}{\partial \beta \partial \lambda} = -(a-1)\sum_{i=1}^{n} \frac{1}{x_i} \cdot \frac{\log(1+\beta/x_i)}{1+\beta/x_i}.$$

and so on, with symmetry ensuring that $\frac{\partial^2 \ell}{\partial \theta_j \partial \theta_k} = \frac{\partial^2 \ell}{\partial \theta_k \partial \theta_j}$. Once the observed Fisher information matrix $\hat{\mathcal{I}}(\hat{\boldsymbol{\theta}})$ is evaluated at the MLEs, its inverse provides the estimated asymptotic covariance matrix of the parameter estimates, that is

$$\mathrm{Cov}(\hat{\boldsymbol{\theta}}) = \hat{\mathcal{I}}(\hat{\boldsymbol{\theta}})^{-1}.$$

From this covariance matrix, one can compute the standard errors of the MLEs as the square roots of its diagonal elements, and approximate confidence intervals for each parameter are then obtained through the normal approximation as

$$\hat{\theta}_j \pm z_{\gamma/2} \cdot \mathrm{SE}(\hat{\theta}_j),$$

where $z_{\gamma/2}$ denotes the upper $\gamma/2$ quantile of the standard normal distribution. It is worth noting that the accuracy of these MLE-based confidence intervals improves with increasing sample size, while for small samples, resampling techniques such as the bootstrap can provide more reliable inference.

Thus, to assess the accuracy of the EK–IL parameter estimates via the FIM and its corresponding inverse, we generate a random sample of size $n = 100$ using the EK–IL quantile function and compute the observed FIM at the MLEs. The observed Fisher Information is:

$$\mathbf{I} = \begin{bmatrix} 302.15929 & -86.84864 & -12.10016 & 21.90504 & 18.24984 \\ -86.84864 & 133.20982 & -78.85736 & -151.92310 & -36.53533 \\ -12.10016 & -78.85736 & 242.53061 & -21.16664 & 9.21573 \\ 21.90504 & -151.92310 & -21.16664 & 924.60788 & 31.92418 \\ 18.24984 & -36.53533 & 9.21573 & 31.92418 & 37.08255 \end{bmatrix}.$$

The inverse FIM, which approximates the asymptotic covariance matrix of the MLEs, is:

$$\mathbf{I}^{-1} = \begin{bmatrix} 0.00499 & 0.00625 & 0.00227 & 0.00088 & 0.00238 \\ 0.00625 & 0.02497 & 0.00812 & 0.00357 & 0.01643 \\ 0.00227 & 0.00812 & 0.00683 & 0.00130 & 0.00407 \\ 0.00088 & 0.00357 & 0.00130 & 0.00163 & 0.00136 \\ 0.00238 & 0.01643 & 0.00407 & 0.00136 & 0.03980 \end{bmatrix}.$$

From $\mathbf{I}^{-1}$, we obtain the asymptotic standard errors (square roots of the diagonal entries), summarized in Table 2.

TABLE 2. Asymptotic standard errors of the EK–IL parameter estimates

Parameter	Standard Error (SE)
$\hat{a}$	0.07063
$\hat{b}$	0.15802
$\hat{c}$	0.08267
$\hat{\beta}$	0.04038
$\hat{\lambda}$	0.19950

Table 2 presents the asymptotic standard errors (SEs) of the EK–IL distribution parameters. Smaller SEs indicate higher precision, with parameter β (SE = 0.04038) being the most precisely estimated, while λ (SE = 0.19950) shows the greatest uncertainty. Parameters a, b, and c exhibit moderate SEs, suggesting estimates that are reliable but less stable.

These findings are consistent with the Fisher Information Matrix (FIM). The diagonal elements of $\mathbf{I}$ measure the information about each parameter, with larger values implying greater precision, while the off-diagonal elements capture dependencies among estimators. The positive diagonal entries of $\mathbf{I}^{-1}$ yield finite variance estimates for the MLEs, and the SEs in Table 2 quantify their sampling uncertainty. Furthermore, the magnitudes of the off-diagonal elements of $\mathbf{I}^{-1}$ confirm non-negligible covariances, indicating correlations among parameter estimates.

4.3. **Monte Carlo Simulation Study.** We assess the performance of the MLEs for the parameters a, b, c, β, and λ of the EK–IL distribution using Monte Carlo simulations. The goal is to evaluate the estimators in terms of accuracy, bias, efficiency, and coverage across varying sample sizes. Two parameter configurations are considered: (i) Parameter Set 1 ($a = 2.0$, $b = 1.0$, $c = 1.2$, $\beta = 1.5$, $\lambda = 1.0$) representing a symmetric distribution with moderate tail, and (ii) Parameter Set 2 ($a = 1.2$, $b = 2.0$, $c = 1.5$, $\beta = 1.2$, $\lambda = 1.2$) representing a right-skewed distribution with light tail. The following performance metrics are used: the Mean Parameter Estimate (MPE), Absolute Value of Bias (AVB), Mean Squared Error (MSE), Average Width (AW), and Coverage Probability (CP). These metrics are evaluated over $N = 3000$ replications for sample sizes $n = 25$, 80, 250, 600, 1500, and 3500. Lower values of AVB, MSE, and RMSE indicate greater estimation accuracy, whereas higher CP (ideally close to 0.95) combined with narrower AW reflects more efficient and reliable interval estimation across repeated samples.

TABLE 3. Results of Monte Carlo Simulations for Parameter Set 1 ($a = 2.0$, $b = 1.0$, $c = 1.2$, $\beta = 1.5$, $\lambda = 1.0$) (Symmetric & Moderate Tail)

Parameter	Sample Size	ME	AVB	RMSE	AW	CP
a	$n = 25$	3.5360	1.53595	2.6892	214.9688	0.8901
	$n = 80$	2.5837	0.58375	1.1244	172.8023	0.8553
	$n = 250$	2.1586	0.15865	0.5271	121.3722	0.8713
	$n = 600$	2.0748	0.07478	0.3300	102.0470	0.9262
	$n = 1500$	2.0097	0.00971	0.1221	98.6987	0.9881
	$n = 3500$	2.0001	0.00014	0.0385	84.3739	0.9981
b	$n = 25$	4.1976	3.19763	24.7519	54.2605	0.9101
	$n = 80$	1.0637	0.06370	0.3109	0.9306	0.8845
	$n = 250$	1.0236	0.02364	0.1339	0.5018	0.9411
	$n = 600$	1.0058	0.00581	0.0729	0.3040	0.9423
	$n = 1500$	1.0041	0.00410	0.0463	0.1865	0.9329
	$n = 3500$	1.0008	0.00077	0.0310	0.1239	0.9276
c	$n = 25$	3.6861	2.4861	7.7776	149.2813	0.8564
	$n = 80$	1.7015	0.5015	1.3810	75.1865	0.8099
	$n = 250$	1.1959	0.00406	0.5580	48.9769	0.8453
	$n = 600$	1.1729	0.02706	0.3121	49.2247	0.9007
	$n = 1500$	1.2028	0.00285	0.1644	40.5510	0.9829
	$n = 3500$	1.2017	0.00172	0.0421	39.7281	0.9981
β	$n = 25$	16.4608	14.9608	113.1465	149.3205	0.4280
	$n = 80$	1.4537	0.04626	1.1717	5.6692	0.7185
	$n = 250$	1.6024	0.10237	0.6470	3.3729	0.8945
	$n = 600$	1.5174	0.01742	0.3698	2.0929	0.9238
	$n = 1500$	1.5105	0.01050	0.2498	1.3153	0.9537
	$n = 3500$	1.5008	0.00077	0.1728	0.8786	0.9529
λ	$n = 25$	3.2667	2.2667	3.6813	157.6601	0.8867
	$n = 80$	1.8971	0.8971	1.6457	96.2603	0.8442
	$n = 250$	1.2831	0.2831	0.8466	61.3278	0.8771
	$n = 600$	1.1371	0.1371	0.5451	51.2232	0.9147
	$n = 1500$	1.0249	0.0249	0.2092	47.9074	0.9868
	$n = 3500$	1.0068	0.0068	0.0800	37.7189	0.9983

TABLE 4. Results of Monte Carlo Simulations for Parameter Set 2 ($a = 1.2$, $b = 2.0$, $c = 1.5$, $\beta = 1.2$, $\lambda = 1.2$) (Right-Skewed & Light Tail)

Parameter	Sample Size	ME	AVB	RMSE	AW	CP
a	$n = 25$	2.0648	0.8648	1.8164	208.5631	0.9733
	$n = 80$	1.7340	0.5340	1.4787	134.7889	0.9659
	$n = 250$	1.4775	0.2775	0.9077	74.5923	0.9790
	$n = 600$	1.3477	0.1477	0.5853	48.1044	0.9780
	$n = 1500$	1.2922	0.0922	0.4083	35.6760	0.9873
	$n = 3500$	1.2559	0.0559	0.2717	27.3100	0.9950
b	$n = 25$	325.4534	323.4534	2347.7026	1512.2451	0.8269
	$n = 80$	3.1582	1.1582	7.5396	15.1522	0.9152
	$n = 250$	2.2467	0.2467	0.7847	2.3290	0.9556
	$n = 600$	2.0714	0.0714	0.3185	1.1207	0.9471
	$n = 1500$	2.0353	0.0353	0.1582	0.6688	0.9568
	$n = 3500$	2.0133	0.0133	0.1030	0.4215	0.9498
c	$n = 25$	4.8242	3.3242	12.2234	162.1319	0.8964
	$n = 80$	3.3043	1.8043	7.2344	67.5134	0.8397
	$n = 250$	2.1660	0.6660	3.9153	26.2183	0.8921
	$n = 600$	1.7173	0.2173	1.4624	16.2517	0.9214
	$n = 1500$	1.5575	0.0575	0.7791	12.6566	0.9116
	$n = 3500$	1.4941	0.0059	0.4853	9.5971	0.9391
β	$n = 25$	245.7270	244.5270	1623.3402	783.1979	0.6389
	$n = 80$	5.9903	4.7903	27.7560	111.8551	0.8255
	$n = 250$	2.0567	0.8567	4.9832	14.7373	0.8848
	$n = 600$	1.3144	0.1144	1.2442	5.3315	0.9180
	$n = 1500$	1.2101	0.0101	0.3582	4.3729	0.9207
	$n = 3500$	1.1860	0.0140	0.1972	3.3568	0.9534
λ	$n = 25$	2.0648	0.8648	1.8164	208.5618	0.9733
	$n = 80$	1.7340	0.5340	1.4787	134.7881	0.9659
	$n = 250$	1.4775	0.2775	0.9077	74.5919	0.9790
	$n = 600$	1.3477	0.1477	0.5853	48.1042	0.9780
	$n = 1500$	1.2922	0.0922	0.4083	35.6759	0.9873
	$n = 3500$	1.2559	0.0559	0.2717	27.3100	0.9950

Tables 3 and 4 show that MLEs of EK–IL parameters improve markedly with larger sample sizes. Bias and RMSE decline, confidence intervals shrink, and coverage probabilities approach nominal levels. Small samples, however, yield unstable estimates, especially for β and b. Overall, consistency and efficiency of the estimators are confirmed, with better performance under larger n.

Remark 1. *Simulation results show that estimation is more challenging under Parameter Sets 3 ($a = 4.0$, $b = 1.5$, $c = 2.0$, $\beta = 0.6$, $\lambda = 2.5$) and 4 ($a = 1.5$, $b = 1.5$, $c = 2.0$, $\beta = 0.5$, $\lambda = 0.8$), which represent skewed and heavily dispersed blood loss patterns. For small samples, particularly in estimating c and β, higher bias, RMSE, and poorer coverage probabilities are observed. As sample size increases, these issues diminish, intervals narrow, coverage improves, and estimates converge to their true values, demonstrating the consistency and reliability of maximum likelihood estimation even under extreme tail behavior. The details are withheld here to conserve space.*

5. Real Data Applications

The EK–IL distribution will be used to model the blood loss data of 300 pregnant women who delivered at the University College Hospital (UCH), Ibadan, Nigeria. To further assess and demonstrate the flexibility of this distribution, four additional datasets will also be analyzed and compared with other distributions within the same class.

To evaluate the practical performance of the EK–IL distribution, at least three competing probability distributions (EK–IL inclusive) are fitted to each dataset, chosen for their suitability to the data's structural properties and prior usage in the literature. Model assessment relies on selection criteria (AIC, BIC, CAIC, HQIC) and goodness-of-fit statistics (KS, AD, CVM), complemented by graphical illustrations. Information criteria such as AIC and BIC have been widely employed in the statistical literature (see, e.g., [20,22]). This framework enables a rigorous comparison of EK–IL against alternative distributions, highlighting its ability to capture real-world features such as asymmetry and heavy tails. The following summarize the mathematical forms and characteristics of the competing distributions:

(1) **PDF:**

$$f(x;\alpha,\beta,\lambda) = \lambda e^{-\lambda x}\,\mathrm{BetaPDF}(1-e^{-\lambda x};\alpha,\beta), \quad x \geq 0,$$

$\alpha, \beta > 0$, $\lambda > 0$.

(2) **Beta-Weibull Distribution (BetaWeibull)** [19]:
PDF:

$$f(x;a,b,p,q) = abx^{b-1}e^{-ax^b}\,\mathrm{BetaPDF}(1-e^{-ax^b};p,q), \quad x \geq 0,$$

$a, b > 0$, $p, q > 0$.

(3) **Generalized Exponential Distribution (GenExp)** [21]:
PDF:

$$f(x;\alpha,\lambda) = \alpha\lambda e^{-\lambda x}\left(1-e^{-\lambda x}\right)^{\alpha-1}, \quad x \geq 0,$$

$\alpha > 0$, $\lambda > 0$.

(4) **Weibull Power Exponential Distribution (WPE)** [14]:
PDF:

$$f(x;\beta,c,\lambda) = \frac{\beta c}{x}(\log(x/\lambda))^{c-1}\exp[-(\log(x/\lambda))^{c}], \quad x \geq 0,$$

$\beta, c > 0$, $\lambda > 0$.

(5) **PDF:**

$$f(x) = \frac{1}{B(a,b)}\cdot\alpha\lambda e^{-\lambda x}\left(1-e^{-\lambda x}\right)^{\alpha a-1}\left[1-\left(1-e^{-\lambda x}\right)^{\alpha}\right]^{b-1}, \quad x \geq 0,$$

$a, b > 0$, $\alpha, \lambda > 0$.

(6) **Beta Burr Type XII Distribution (BBXII)** [24]:
PDF:

$$f(x;\alpha,\lambda,a,b,c) = \frac{\alpha c\,\Gamma(a+b)}{\lambda\,\Gamma(a)\Gamma(b)}\left(\frac{x}{\lambda}\right)^{\alpha-1}\left(1+\left(\frac{x}{\lambda}\right)^{\alpha}\right)^{-bc-1} \times\left[1-\left(1+\left(\frac{x}{\lambda}\right)^{\alpha}\right)^{-c}\right]^{a-1}, \quad x > 0,$$

$\alpha, \lambda, a, b, c > 0$, where $I_u(a,b)$ is the regularized incomplete Beta function and $B(a,b) = \frac{\Gamma(a)\Gamma(b)}{\Gamma(a+b)}$.

5.1. **Blood Loss During Childbirth.** A total of 300 blood loss measurements (in milliliters) were recorded from pregnant women who delivered at the University College Hospital (UCH), Ibadan, Nigeria [16]. The data were obtained using a simple random sampling method, ensuring that each patient had an equal chance of selection. Blood loss values ranged from 50 ml to 800 ml, capturing the variability among patients and providing a comprehensive overview of the distribution of blood loss during childbirth at UCH.

Exploratory data analysis was performed on the blood loss data to summarize key characteristics and visualize the distribution. The summary statistics and graphical representations are presented in Table 5 and Figure 7.

TABLE 5. Summary Statistics of Blood Loss (ml)

Statistic	Min	1st Qu.	Median	Mean	3rd Qu.	Max	SD	Variance	IQR	Skewness	Kurtosis
Value	50	100	250	271.5	400	800	168.95	28543.23	300	0.73	-0.13

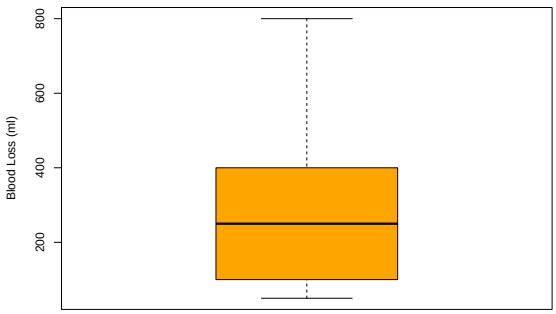

FIGURE 5. *
(a) Boxplot of Blood Loss

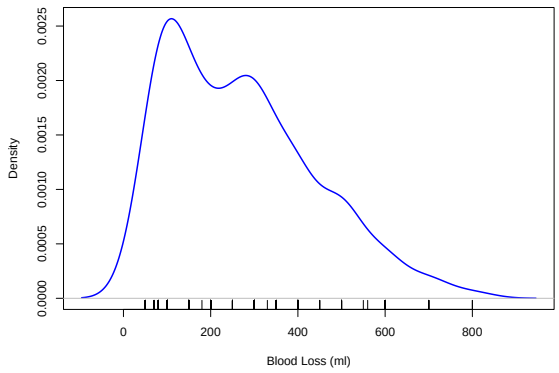

FIGURE 6. *
(b) Density Plot of Blood Loss

FIGURE 7. Visual summary of the blood loss measurements (ml) of pregnant women at UCH Ibadan.

Table 5 presents the descriptive statistics for blood loss (ml) based on a sample of 300 observations from the study population. The mean blood loss is 271.5 ml, while the median is 250 ml, reflecting a slightly right-skewed distribution, further supported by a skewness value of 0.73. The variability in blood loss is notable, with a standard deviation of 168.95 ml and an interquartile range of 300 ml. As shown in Figure 7(a), a few potential outliers appear above 400 ml, and Figure 7(b) depicts a unimodal distribution with a mild right tail. Taken together, these findings indicate moderate variability and a slight positive skew in blood loss across the study sample.

TABLE 6. Parameter Estimates and Goodness-of-Fit Statistics for Fitted Models for the Blood Loss Measurements (ml) of Pregnant Women at UCH Ibadan

Statistic	EK–IL	BetaWeibull	BGE	GenExp	BetaExp	BBXII	WPE
Parameter Estimates							
$\hat{a}$	11.4017	0.0200	0.7733	–	–	62.3748	0.2440
$\hat{b}$	18.3248	0.7733	0.0200	–	–	71.2758	6.5378
$\hat{c}$	0.1381	–	–	–	–	100.0149	4.8233
$\hat{\beta}$	14.0693	–	–	–	0.9998	–	–
$\hat{\lambda}$	11.4017	–	–	0.0064	0.0065	0.6204	–
$\hat{\alpha}$	–	–	–	2.6914	2.7477	0.2568	–
$\hat{p}$	–	4.2764	4.2764	–	–	–	–
$\hat{q}$	–	1.7315	1.7315	–	–	–	–
Model Selection Metrics & Goodness-of-Fit Statistics							
AIC	3855.94	3866.60	3866.60	3861.58	3863.71	3877.67	3858.05
BIC	3874.46	3881.42	3881.42	3868.99	3874.83	3896.19	3869.17
CAIC	3879.46	3885.42	3885.42	3870.99	3877.83	3901.19	3872.17
HQIC	3863.35	3872.53	3872.53	3864.54	3868.16	3885.08	3862.50
Log Likelihood	-1922.97	-1929.30	-1929.30	-1928.79	-1928.86	-1933.83	-1926.03
K-S Statistic	0.1227	0.1302	0.1302	0.1300	0.1306	0.1367	0.1333
AD Statistic	8.3781	9.1914	9.1914	8.9835	9.1532	10.1077	8.8303
Cramér–von Mises Statistic	0.6019	0.6778	0.6778	0.6335	0.6857	0.8925	0.6354

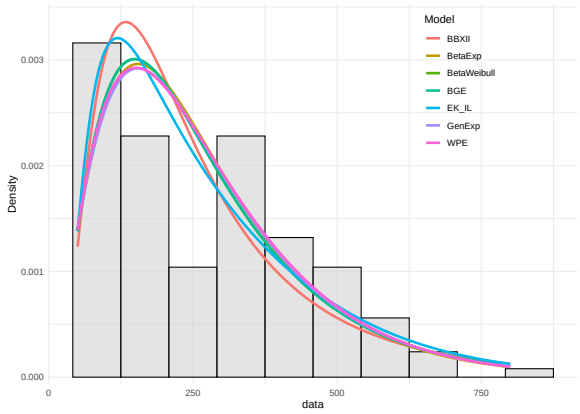

FIGURE 8. *
(a) Histogram and Fitted PDFs

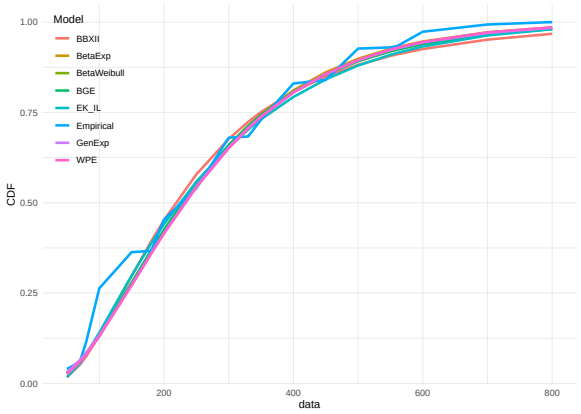

FIGURE 9. *
(b) Empirical vs Fitted CDFs

FIGURE 10. Comparison of fitted probability density and cumulative distribution functions across models for the Blood Loss Measurements (ml) of Pregnant Women at UCH Ibadan.

The maternal blood loss dataset from pregnant women at UCH Ibadan was evaluated using parameter estimates, goodness-of-fit statistics (Table 9), and visual comparisons of fitted probability density and cumulative distribution functions (Figure 10). Among the competing models, the EK–IL distribution provided the best overall fit, with the lowest AIC (3855.94), BIC (3874.46), HQIC (3863.35), and the highest log-likelihood (–1922.97). It outperformed the BetaWeibull, BGE, GenExp, BetaExp, BBXII, and WPE alternatives, with the latter performing competitively but slightly less effectively.

Clinically, this indicates that the EK–IL model most accurately represents the distribution of maternal blood loss, particularly its long right-tail, which corresponds to women experiencing excessive or atypical bleeding, a critical determinant of obstetric risk.

Goodness-of-fit tests reinforce this conclusion. The Kolmogorov–Smirnov (K–S) statistic for EK–IL (0.1227) was lower than those of all competing models, while its Anderson–Darling (8.3781) and Cramér–von Mises (0.6019) statistics were also smaller, confirming closer alignment with the observed distribution.

Graphical comparisons further validate the model. The EK–IL fitted PDF closely tracks the histogram of blood loss, especially in the high-loss region, while its CDF aligns tightly with the empirical CDF.

Overall, the EK–IL distribution emerges as both statistically robust and clinically relevant, offering a reliable framework for modeling maternal blood loss and supporting improved risk assessment and decision-making in maternal health care section at UCH.

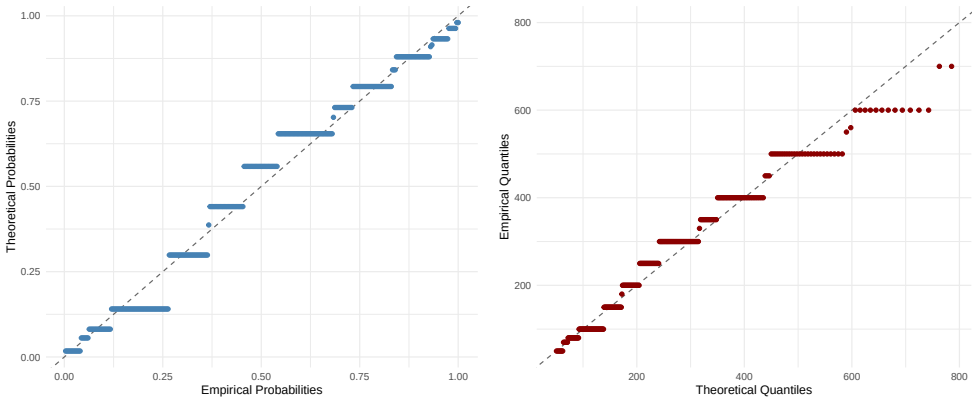

FIGURE 11. PP (left) and QQ (right) plots for EK–IL model for the Blood Loss Measurements (ml) of Pregnant Women at UCH Ibadan.

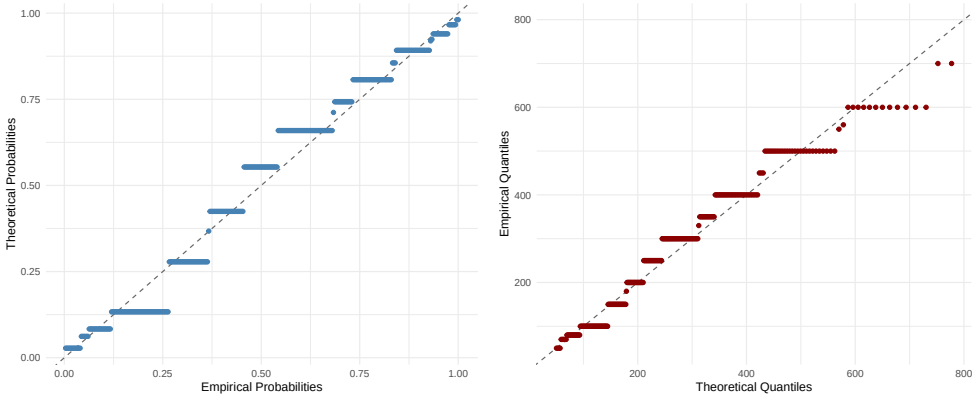

FIGURE 12. PP (left) and QQ (right) plots for BetaWeibull model for the Blood Loss Measurements (ml) of Pregnant Women at UCH Ibadan.

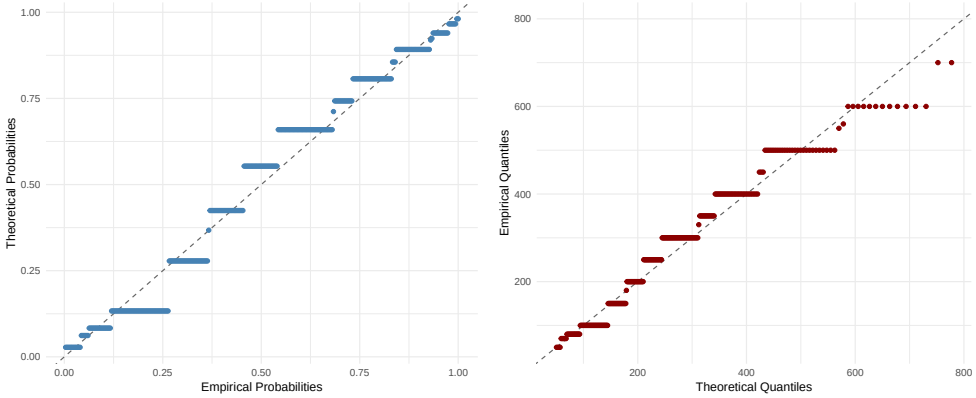

FIGURE 13. PP (left) and QQ (right) plots for BGE model for the Blood Loss Measurements (ml) of Pregnant Women at UCH Ibadan.

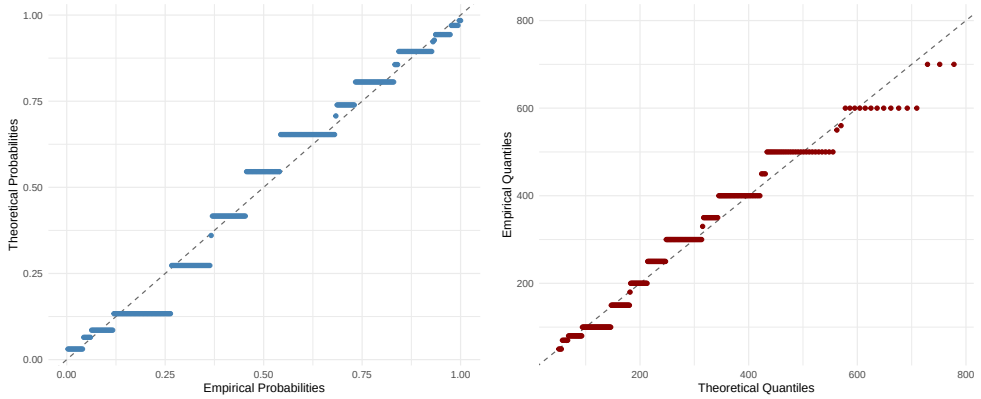

FIGURE 14. PP (left) and QQ (right) plots for GenExp model for the Blood Loss Measurements (ml) of Pregnant Women at UCH Ibadan.

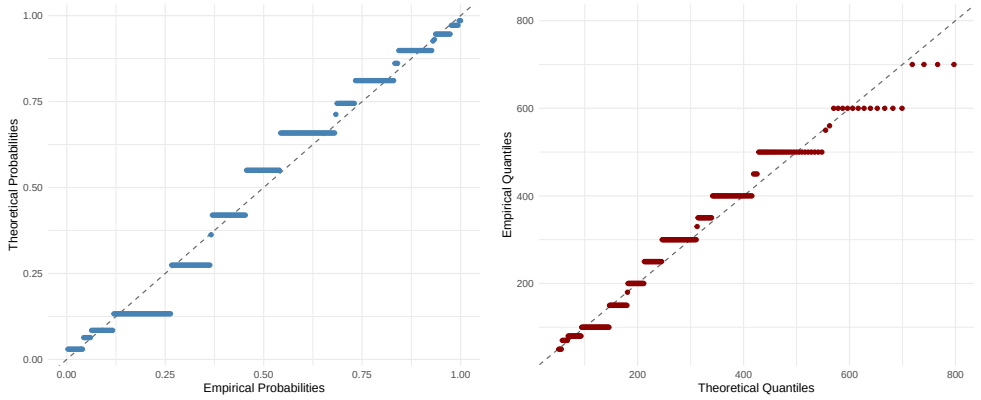

FIGURE 15. PP (left) and QQ (right) plots for BetaExp model for the Blood Loss Measurements (ml) of Pregnant Women at UCH Ibadan.

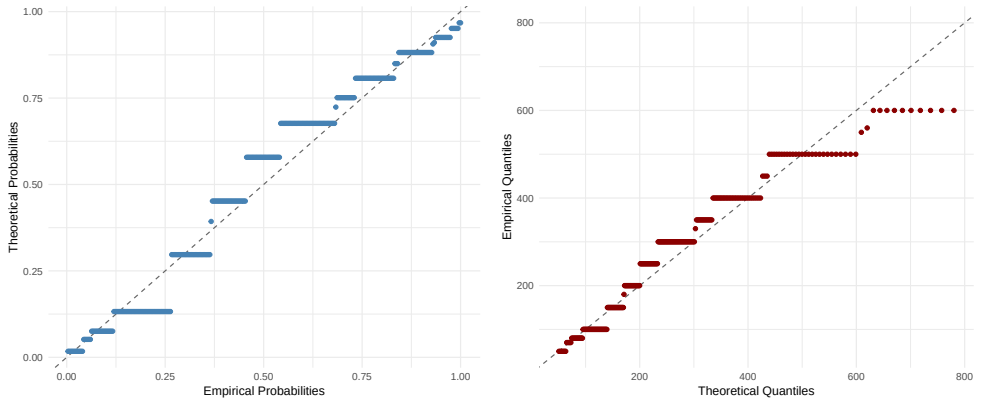

FIGURE 16. PP (left) and QQ (right) plots for BBXII model for the Blood Loss Measurements (ml) of Pregnant Women at UCH Ibadan.

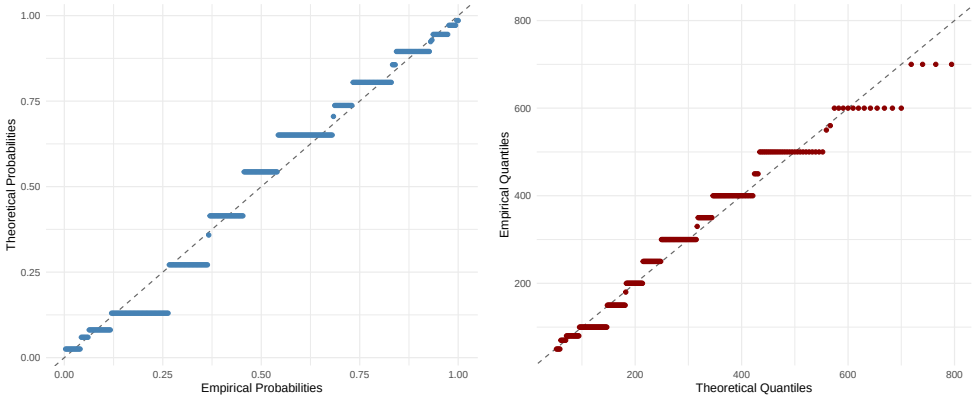

FIGURE 17. PP (left) and QQ (right) plots for WPE model for the Blood Loss Measurements (ml) of Pregnant Women at UCH Ibadan.

The PP and QQ plots shown in Figures 11–17 provide additional diagnostic validation of model performance for the blood loss dataset. The EK–IL distribution demonstrates points that align more closely with the reference diagonal in both plots, indicating a superior ability to capture the observed data distribution. In contrast, the BetaWeibull, BGE, GenExp, BetaExp, BBXII, and WPE models exhibit greater deviations, most notably in the tails, suggesting reduced accuracy in modeling extreme blood loss values. Collectively, these findings support the EK–IL model as the most clinically reliable representation of perioperative blood loss.

5.2. **Fatigue Time of 101 6061-T6 Aluminum Coupons.** The second dataset, as reported by [14], consists of fatigue life measurements (in cycles) for 101 6061-T6 aluminum coupons, ranging from 70 to 212 cycles.

Most observations in the dataset are concentrated between 100 and 160 cycles, with a mean fatigue life of 132.3 cycles and a median of 131 cycles, indicating slight positive skewness. The interquartile range of 34 cycles and a standard deviation of 21.9 cycles reflect moderate variability in fatigue times. A skewness value of 1.01 confirms a right-skewed distribution, while a kurtosis of 3.92 suggests mildly heavier tails, indicating the presence of occasional extreme fatigue lives. Overall, the majority of coupons exhibit fatigue times between 114 and 148 cycles, with a few high-end outliers contributing to the observed dispersion.

TABLE 7. Parameter Estimates and Goodness-of-Fit Statistics for Fitted Models for Fatigue Time of 101 6061-T6 Aluminum Coupons

Statistic	EK–IL	BetaWeibull	BGE	GenExp	BBXII
Parameter Estimates					
α	–	–	–	286.5074	0.7659282
$\hat{a}$	5.542190	0.008276	1.258664	–	151.2205
$\hat{b}$	219.4077	1.258664	0.008276	–	144.9408
$\hat{c}$	1.940763	–	–	–	26.52546
$\hat{\beta}$	24.54945	–	–	–	–
$\hat{\lambda}$	5.542190	–	–	0.04608584	2.922261
$\hat{p}$	–	32.72180	32.72180	–	–
$\hat{q}$	–	0.9788265	0.9788265	–	–
Model Selection Metrics & Goodness-of-Fit Statistics					
AIC	922.0238	941.3618	941.3618	929.2254	924.6833
BIC	935.0994	951.8223	951.8223	934.4556	937.7589
CAIC	940.0994	955.8223	955.8223	936.4556	942.7589
HQIC	927.3172	945.5965	945.5965	931.3427	929.9767
Log Likelihood	-456.0119	-466.6809	-466.6809	-462.6127	-457.3417
K-S Statistic	0.0658	0.1310	0.1310	0.1088	0.0865
AD Statistic	1.0210	0.6112	0.6112	1.1376	1.0983
Cramér-von Mises Statistic	0.0507	0.5064	0.5064	0.2229	0.0893

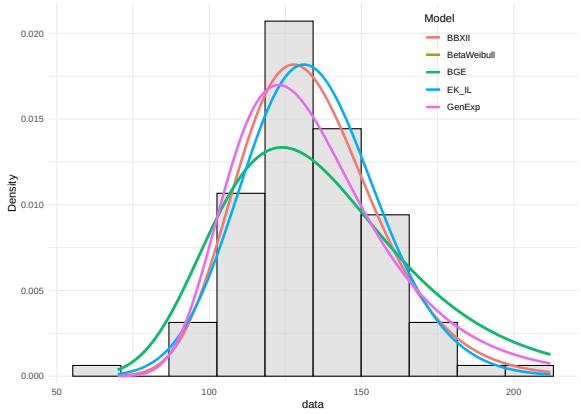

FIGURE 18. *
(a) Histogram and Fitted PDFs

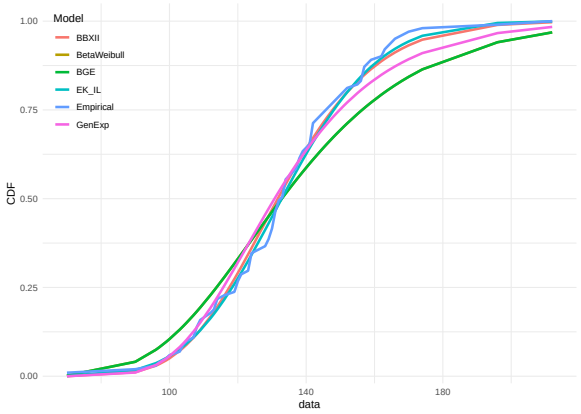

FIGURE 19. *
(b) Empirical vs Fitted CDFs

FIGURE 20. Comparison of fitted probability density and cumulative distribution functions across models for Fatigue Time of 101 6061-T6 Aluminum Coupons.

The fatigue time data for 101 6061-T6 aluminum coupons were modeled using five candidate distributions, with parameter estimates and goodness-of-fit statistics reported in Table 9. Among

the models, the EK–IL distribution provides the most satisfactory fit, achieving the lowest AIC (922.02), BIC (935.10), and HQIC (927.32), alongside the highest log-likelihood (−456.01). The BBXII distribution also performs competitively, with slightly higher information criteria but still better than the BetaWeibull, BGE, and GenExp models.

Goodness-of-fit test results further highlight EK–IL as a superior choice. It records the smallest K-S statistic (0.0658), indicating closer agreement with the observed data. In comparison, BetaWeibull and BGE show larger deviations (K-S = 0.1310). Similarly, the Cramér–von Mises test favors EK–IL, whereas other models fail to capture the data adequately. Although the Anderson–Darling test suggests some departure from the data, such results are common for heavy-tailed datasets.

Figure 20 supports these findings, where the EK–IL fitted PDF closely follows the fatigue time histogram and its CDF aligns with the empirical distribution. Overall, EK–IL best characterizes the fatigue behavior of the aluminum coupons.

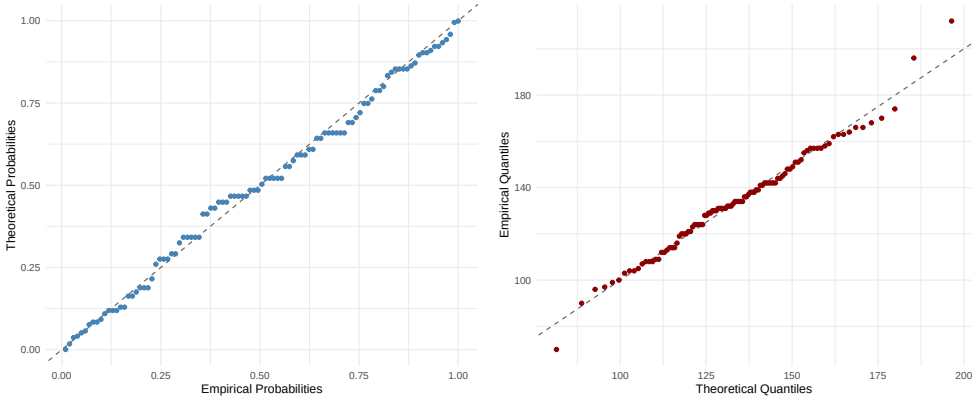

FIGURE 21. PP (left) and QQ (right) plots for EK–IL model for Fatigue Time of 101 6061-T6 Aluminum Coupons.

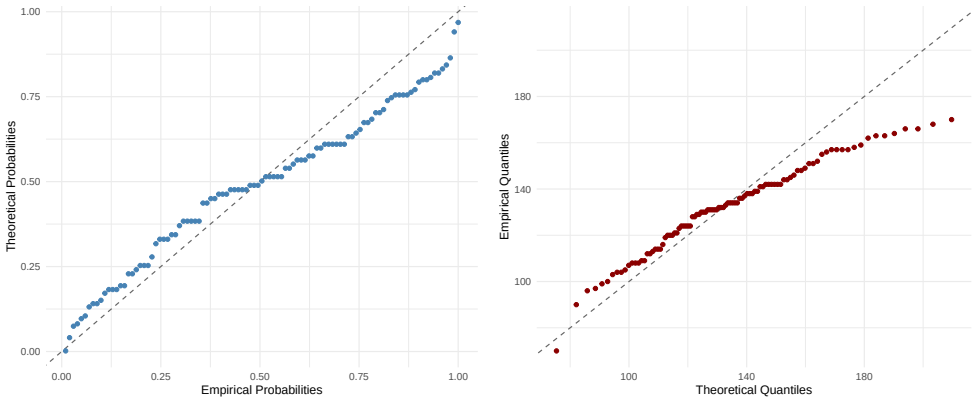

FIGURE 22. PP (left) and QQ (right) plots for BetaWeibull model for Fatigue Time of 101 6061-T6 Aluminum Coupons.

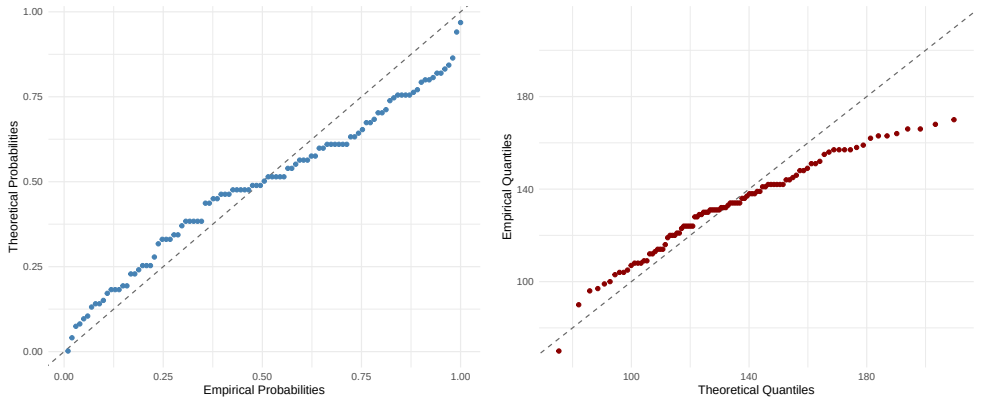

FIGURE 23. PP (left) and QQ (right) plots for BGE model for Fatigue Time of 101 6061-T6 Aluminum Coupons.

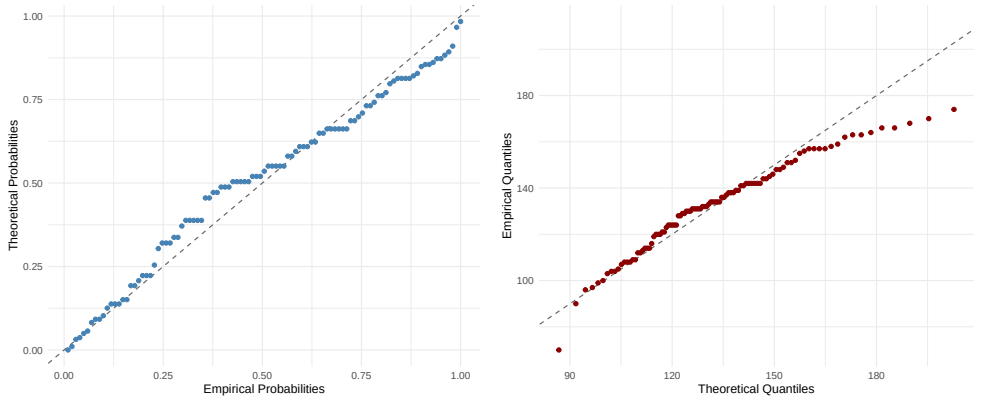

FIGURE 24. PP (left) and QQ (right) plots for GenExp model for Fatigue Time of 101 6061-T6 Aluminum Coupons.

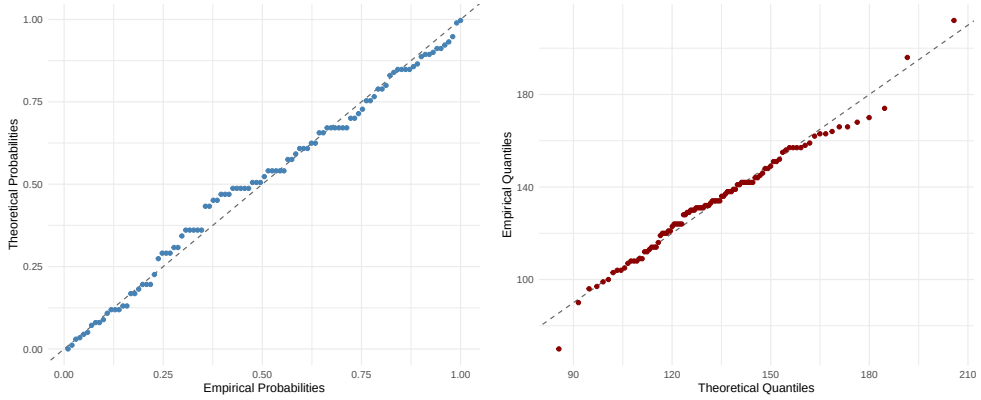

FIGURE 25. PP (left) and QQ (right) plots for BBXII model for Fatigue Time of 101 6061-T6 Aluminum Coupons.

The PP and QQ plots in Figures 29–37 provide visual diagnostics of model adequacy for the fatigue time data. The EK–IL model shows points that lie closest to the 45-degree reference line, particularly in the central range, indicating its strong agreement with the empirical distribution. In contrast, BetaWeibull, BGE, and GenExp exhibit clear departures from the diagonal, especially in the tails, suggesting poorer fit. The BBXII model performs moderately well but remains inferior to EK–IL. Overall, the plots reinforce EK–IL as the most suitable model.

5.3. **Life Span of Batteries Data.** The third dataset, obtained from [13], contains the lifespans (in years) of 40 batteries, ranging from 1.6 to 4.7 years. Based on the observed battery lifespan data, the mean lifespan is 3.47 years and the median is 3.4 years, indicating slight right skewness. Most lifespans are concentrated between 3.1 and 3.8 years, as indicated by an interquartile range of 0.7 years, while a standard deviation of 0.70 years reflects moderate variability. A skewness value of 0.22 indicates that the distribution is nearly symmetric, and a kurtosis of 2.65 suggests slightly lighter tails than those of a normal distribution. Overall, battery lifespans appear fairly consistent, with few extreme values.

TABLE 8. Parameter Estimates and Goodness-of-Fit Statistics for Selected Models for the Life Span of Batteries (in years)

Statistic	EK–IL	GenExp	BetaExp
Parameter Estimates			
$\hat{a}$	4.6398	–	–
$\hat{b}$	12754	–	–
$\hat{c}$	0.5455	–	–
$\hat{\beta}$	2.1901	–	0.0945
$\hat{\lambda}$	4.6398	57.5939	57.2385
$\hat{\alpha}$	–	57.5939	21.5856
Model Selection Metrics & Goodness-of-Fit Statistics			
AIC	93.64	99.37	93.88
BIC	102.08	102.75	98.95
CAIC	107.08	104.75	101.95
HQIC	96.69	100.59	95.72
LogLik	-41.82	-47.69	-43.94
K-S Statistic	0.0959	0.1701	0.1324
AD Statistic	0.4075	0.4215	0.3565
Cramér–von Mises Statistic	0.0560	0.2024	0.0850

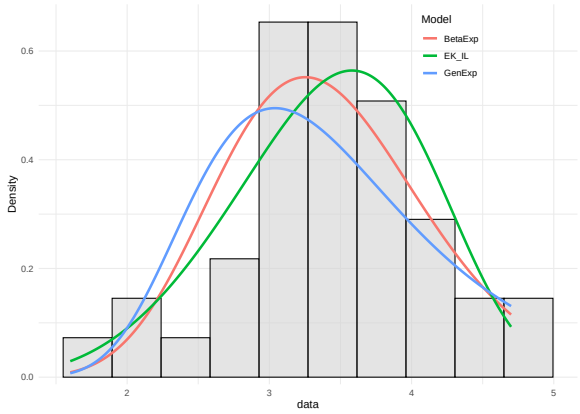

FIGURE 26. *
(a) Histogram and Fitted PDFs

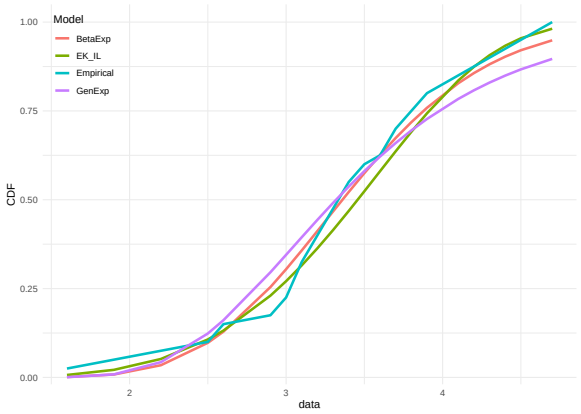

FIGURE 27. *
(b) Empirical vs Fitted CDFs

FIGURE 28. Comparison of fitted probability density and cumulative distribution functions across models for the Life Span of Batteries (in years).

The fitted models for the battery life data were assessed using parameter estimates and goodness-of-fit statistics (Table 9) together with visual inspection of fitted probability density and cumulative distribution functions (Figure 40). Among the candidate models, the EK–IL distribution achieved the best overall performance, yielding the lowest AIC (93.64), HQIC (96.69), and highest log-likelihood (–41.82). Although the BetaExp model displayed a comparable AIC (93.88), its higher BIC and less favorable likelihood suggest that EK–IL provides a more parsimonious fit. The GenExp model was clearly inferior, with substantially larger information criteria values and a poorer likelihood.

In terms of goodness-of-fit tests, the EK–IL model achieved the smallest K–S statistic (0.0959), indicating excellent agreement with the observed data. The AD and Cramér–von Mises statistics further confirmed this result, both yielding low values. The BetaExp model also showed reasonable adequacy, while GenExp deviated more strongly. Visually, Figure 40(a) shows EK–IL tracking the histogram closely, while Figure 40(b) demonstrates its fitted CDF aligning tightly with the empirical CDF. Thus, EK–IL is the most reliable distribution for modeling battery lifespan.

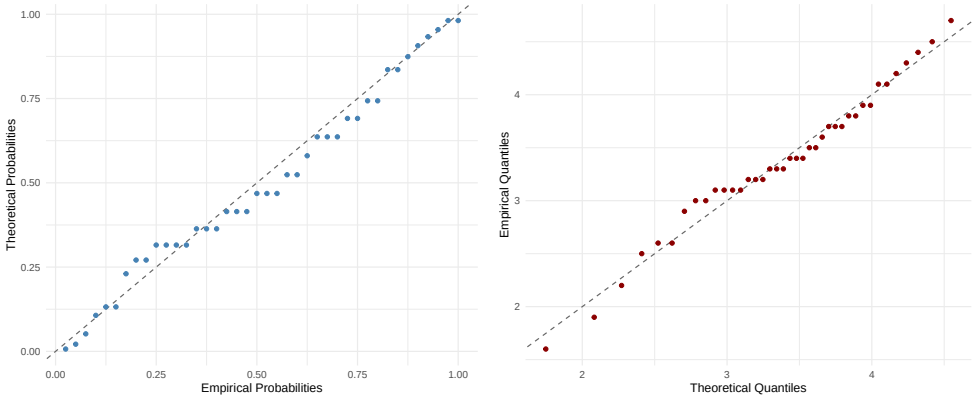

FIGURE 29. PP (left) and QQ (right) plots for EK–IL model for the Life Span of Batteries (in years).

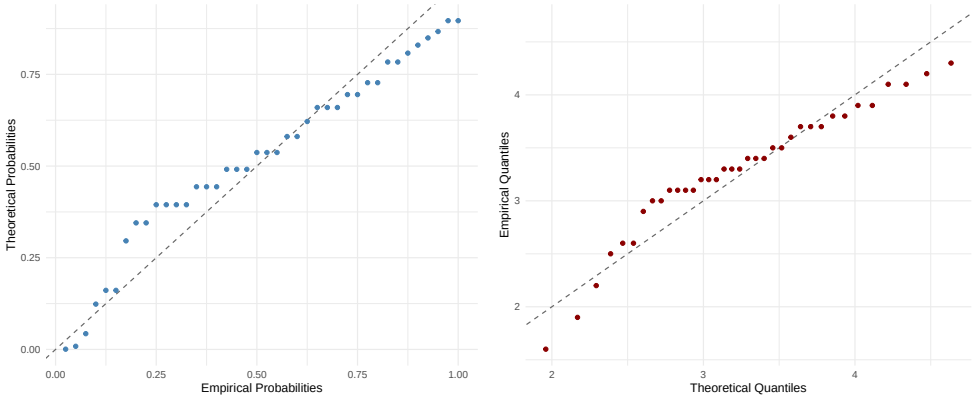

FIGURE 30. PP (left) and QQ (right) plots for GenExp model for the Life Span of Batteries (in years).

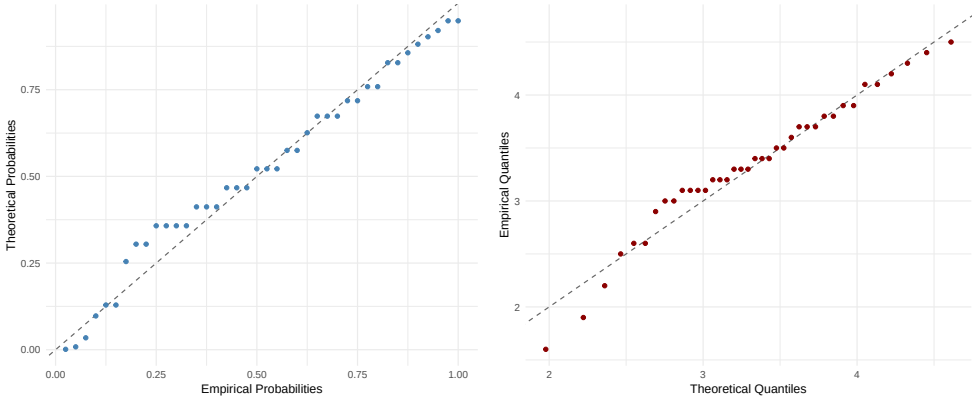

FIGURE 31. PP (left) and QQ (right) plots for BetaExp model for the Life Span of Batteries (in years).

The PP and QQ plots in Figures 29–31 provide further insight into the adequacy of the fitted models for the battery life data. The EK–IL model shows points closely aligned with the diagonal in both PP and QQ plots, confirming its superior fit as indicated in Table 9. In contrast, the GenExp model exhibits systematic deviations from the reference line, reflecting its weaker performance. The BetaExp model demonstrates moderate alignment, performing better than GenExp but inferior to EK–IL, consistent with statistical criteria.

5.4. **Number of Written Words Without Mistakes in Every 100 Words by Students.** The fourth dataset, sourced from [13], represents the number of correctly written words per 100 in students' essays. Based on the observed data, an average of 79.7 words were error-free, with a median of 80, indicating relatively consistent performance. Scores ranged from 58 to 97, with most values concentrated between 74 and 86 (IQR = 12). The distribution is approximately symmetric (skewness = -0.09) and slightly platykurtic (kurtosis = -0.48), suggesting limited extreme deviations in writing accuracy among the students.

TABLE 9. Parameter Estimates and Goodness-of-Fit Statistics for Selected Models for the Number of Written Words Without Mistakes in Every 100 Words by Students

Statistic	EK–IL	GenExp	BBXII
Parameter Estimates			
$\hat{a}$	3.578	-	1.484
$\hat{b}$	2610.620	-	86.060
$\hat{c}$	3.704	-	74.784
$\hat{\beta}$	61.087	-	96.732
$\hat{\lambda}$	3.578	0.121	0.903
$\hat{\alpha}$	-	9473.951	-
Model Selection Metrics & Goodness-of-Fit Statistics			
AIC	464.33	467.62	465.22
BIC	475.12	471.94	476.01
CAIC	480.12	473.94	481.01
HQIC	468.58	469.33	469.47
LogLik	-227.16	-231.81	-227.61
K-S Statistic	0.0763	0.1009	0.0796
AD Statistic	1.0837	1.2662	1.1304
Cramér–von Mises Statistic	0.0373	0.1272	0.0508

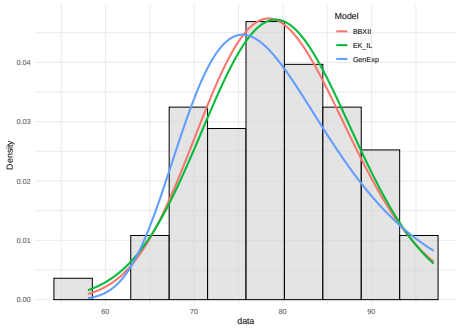

FIGURE 32. *
(a) Histogram and Fitted PDFs

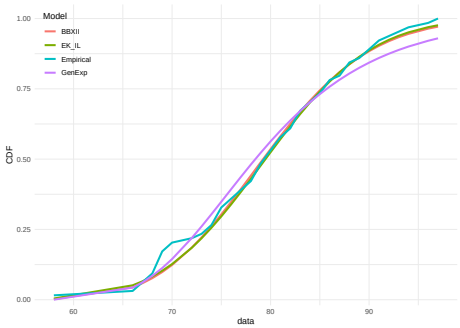

FIGURE 33. *
(b) Empirical vs Fitted CDFs

FIGURE 34. Comparison of fitted probability density and cumulative distribution functions across models for the Number of Written Words Without Mistakes in Every 100 Words by Students.

Table 9 and Figure 40 summarize the parameter estimates and goodness-of-fit performance of the EK–IL, GenExp, and BBXII models for the dataset on the number of written words without mistakes in every 100 words by students. From the table, the EK–IL distribution achieved the lowest AIC (464.33), BIC (475.12), and HQIC (468.58), alongside the highest log-likelihood (−227.16), suggesting that it provides the best overall fit among the candidate models. In addition, EK–IL exhibited the smallest Kolmogorov–Smirnov statistic (0.0763) and the most favorable Cramér–von Mises statistic (0.0373), confirming its strong alignment with the empirical data. Although the Anderson–Darling statistic was relatively large, EK–IL still outperformed GenExp and BBXII across most diagnostic measures. Figure 40(a) shows that the fitted EK–IL PDF tracks the histogram of the dataset more closely than its competitors, while Figure 40(b) demonstrates its CDF closely follows the empirical distribution. Overall, the analysis indicates that EK–IL is the most suitable model for representing students' writing accuracy compared to GenExp and BBXII.

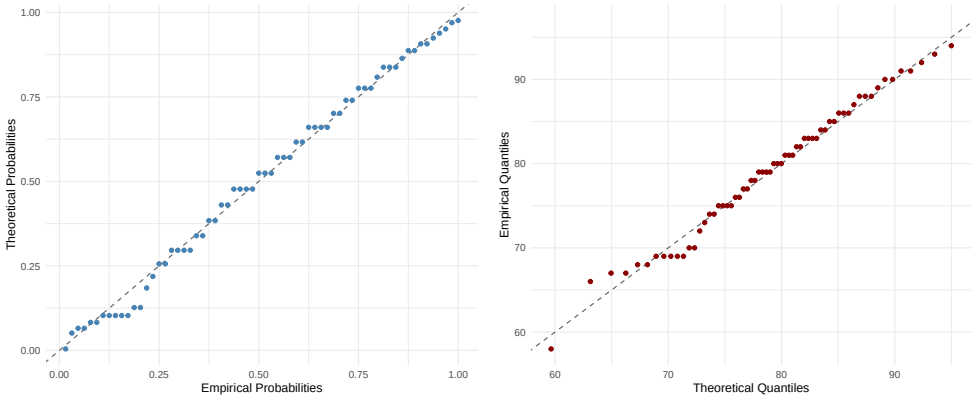

FIGURE 35. PP (left) and QQ (right) plots for EK–IL model for the Number of Written Words Without Mistakes in Every 100 Words by Students.

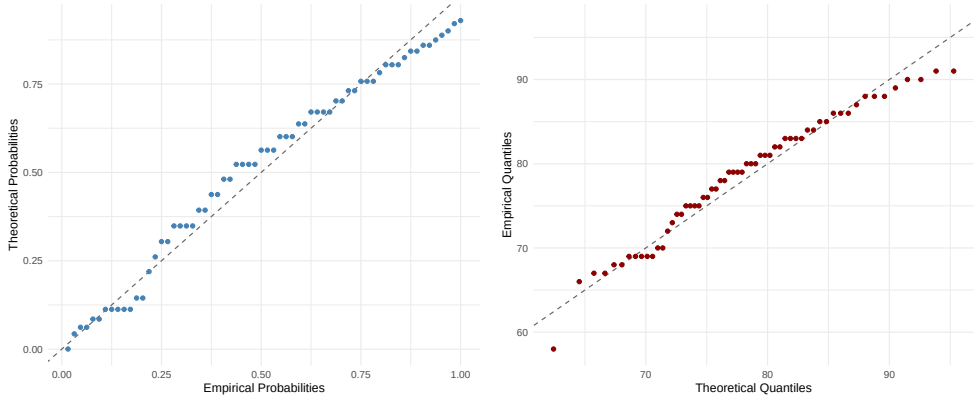

FIGURE 36. PP (left) and QQ (right) plots for GenExp model for the Number of Written Words Without Mistakes in Every 100 Words by Students.

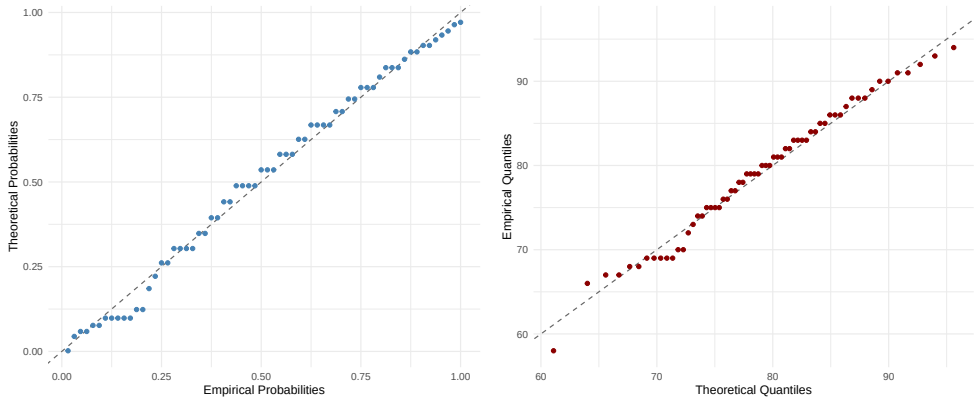

FIGURE 37. PP (left) and QQ (right) plots for BBXII model for the Number of Written Words Without Mistakes in Every 100 Words by Students.

Figures 35–37 present the PP and QQ plots for the EK–IL, GenExp, and BBXII models fitted to the dataset on the number of written words without mistakes in every 100 words by students. The EK–IL plots show points aligning more closely with the 45-degree reference line, indicating superior fit compared to GenExp and BBXII. In contrast, GenExp and BBXII display noticeable deviations, particularly in the tails, reflecting weaker performance. Thus, the diagnostic plots reinforce EK–IL as the most suitable model for the dataset.

5.5. **Carbon Fibre Data.** The fifth dataset, obtained from [12], contains load measurements (in kN) from tensile tests on unidirectional carbon fibre composites. The observed loads range from nearly zero to 4.05 kN, with most values clustered below 2 kN, reflecting typical experimental loads, while higher measurements capture the maximum tensile response before failure. For $n = 65$, the mean load is 1.954 kN and the median 1.7766 kN, indicating slight positive skewness (0.38). Moderate dispersion is indicated by a standard deviation of 1.187 kN, variance of 1.410 kN^2, and a coefficient of variation of 60.7%. The kurtosis of -0.52 suggests a slightly platykurtic distribution.

TABLE 10. Parameter Estimates and Goodness-of-Fit Statistics for Selected Models for the Carbon Fibre Data

Statistic	EK–IL	GenExp	BetaExp
Parameter Estimates			
$\hat{a}$	2.1189	–	–
$\hat{b}$	25409.35	–	–
$\hat{c}$	0.7421	–	–
$\hat{\beta}$	28.0441	–	–
$\hat{\lambda}$	2.1189	1.0076	–
$\hat{\alpha}$	–	9.1992	7.5009
$\hat{\beta}$	–	–	37.6423
$\hat{\lambda}$	–	–	0.0667
Model Selection Metrics & Goodness-of-Fit Statistics			
AIC	182.01	194.74	188.37
BIC	192.96	199.12	194.94
CAIC	197.96	201.12	197.94
HQIC	186.34	196.48	190.97
LogLik	-86.01	-95.37	-91.19
K-S Statistic	0.0848	0.1550	0.1330
AD Statistic	0.5973	1.2561	1.0942
Cramér–von Mises Statistic	0.0875	0.3732	0.2470

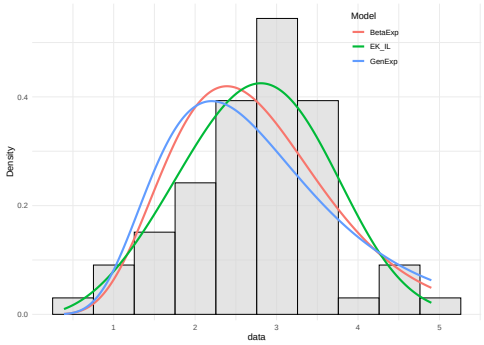

FIGURE 38. *
(a) Histogram and Fitted PDFs

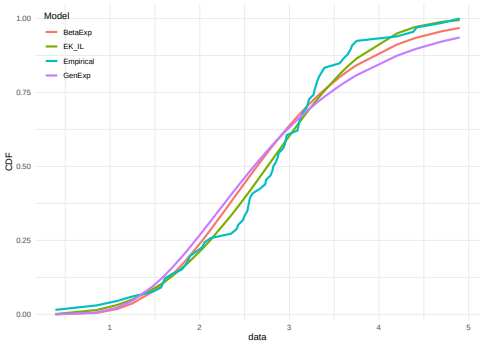

FIGURE 39. *
(b) Empirical vs Fitted CDFs

FIGURE 40. Comparison of fitted probability density and cumulative distribution functions across EK–IL, GenExp, and BetaExp models for the Carbon Fibre Data.

Table 10 and Figure 40 present the parameter estimates and goodness-of-fit results for the EK–IL, GenExp, and BetaExp models fitted to the Carbon Fibre dataset. The EK–IL model provided the best overall fit, with the lowest AIC (182.01), BIC (192.96), and HQIC (186.34), as well as the highest log-likelihood (−86.01). In contrast, the GenExp and BetaExp models showed higher information criteria values, reflecting relatively poorer performance. In terms of goodness-of-fit tests, the EK–IL model achieved the smallest Kolmogorov–Smirnov statistic (0.0848), indicating closer alignment with the observed data. Its Anderson–Darling and Cramér–von Mises statistics were also more favorable than those of the competing models, reinforcing its superiority. Visually, Figure 40(a) shows that the EK–IL fitted density aligns closely with the histogram of the Carbon Fibre data, while Figure 40(b) demonstrates that its CDF tracks the empirical distribution more accurately. Overall, both numerical and graphical assessments establish EK–IL as the most suitable model for describing the Carbon Fibre dataset, outperforming GenExp and BetaExp.

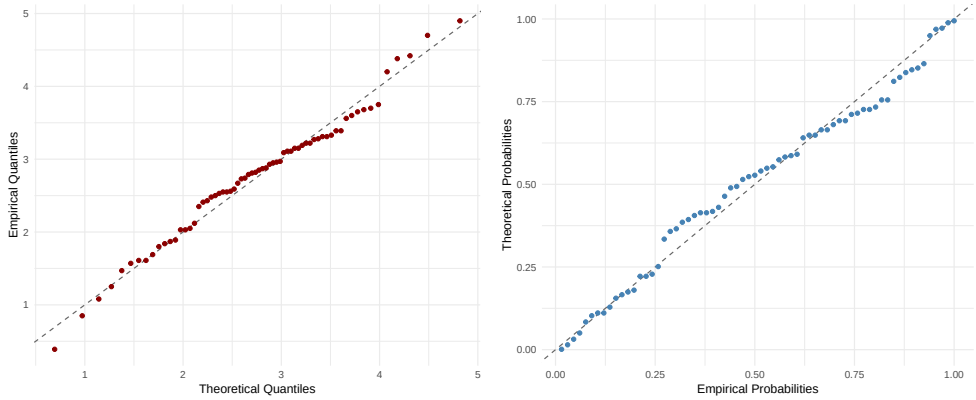

FIGURE 41. QQ (left) and PP (right) plots for EK–IL distribution for the Carbon Fibre Data.

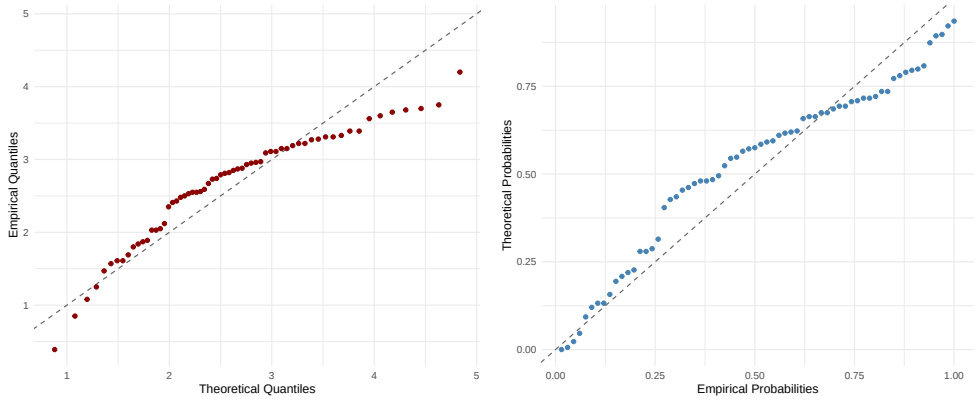

FIGURE 42. QQ (left) and PP (right) plots for the GenExp distribution for the Carbon Fibre Data.

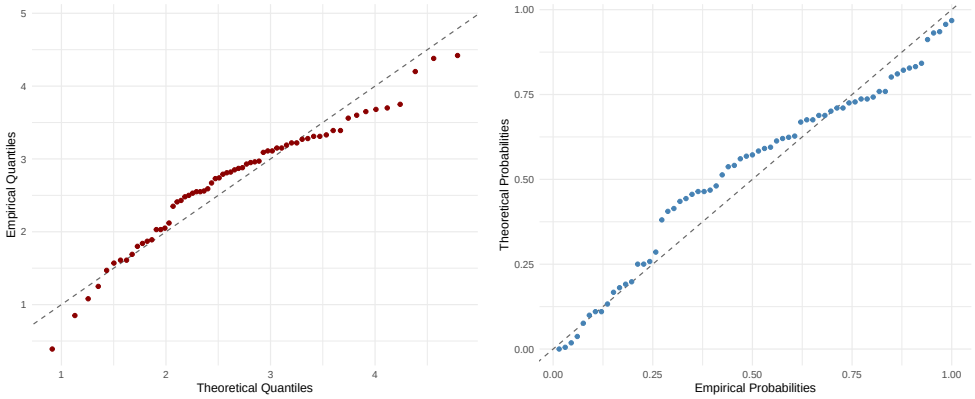

FIGURE 43. QQ (left) and PP (right) plots for the BetaExp distribution for the Carbon Fibre Data.

Figures 41–43 display the QQ and PP plots for the EK–IL, GenExp, and BetaExp models fitted to the Carbon Fibre dataset. The EK–IL model shows points closely aligned with the reference line in both plots, indicating an excellent fit across the distribution. In contrast, the GenExp and BetaExp models exhibit clear deviations, especially in the tails, reflecting weaker performance. These diagnostic plots confirm that the EK–IL distribution provides the most accurate representation of the Carbon Fibre data, consistent with earlier goodness-of-fit results.

6. Summary and Conclusion

A new and flexible probability distribution, the Exponentiated Kumaraswamy–Inverse Lomax (EK–IL) distribution, was introduced and thoroughly investigated in this study. The proposed distribution was applied to model blood loss data from 300 pregnant women who delivered at the University College Hospital (UCH), Ibadan, Nigeria. To further illustrate its adaptability, four additional datasets were analyzed and compared against other distributions in the same class. The results demonstrated that the EK–IL distribution consistently provided superior fits across these datasets, outperforming competing models in both statistical measures and graphical assessments. Given its flexibility and robustness, the EK–IL distribution was expected to find broader applications in modeling diverse real-world data.

Ethics Approval. The authors gratefully acknowledge the Ethics Committee of the University of Ibadan / University College Hospital (UI/UCH), Ibadan, Nigeria, for granting ethical approval for this study (Approval No.: UI/EC/2023/0411). All procedures were carried out in accordance with ethical standards recommended by the journal and global best practices.

Data Availability. All datasets analyzed in this study are available from the corresponding author upon reasonable request.

Code Availability. The R codes used in the analysis are available upon reasonable request from the corresponding author.

Competing interests: The authors declare that there is no conflict of interest regarding the publication of this paper.

References

[1] F. Provost, T. Fawcett, Data Science for Business: What You Need to Know about Data Mining and Data-Analytic Thinking, O'Reilly Media, Inc., Sebastopol, California, 2013. https://www.oreilly.com/library/view/data-science-for/9781449374273.

[2] N. Eugene, C. Lee, F. Famoye, Beta-Normal Distribution and Its Applications, Commun. Stat. - Theory Methods 31 (2002), 497–512. https://doi.org/10.1081/STA-120003130.

[3] A. Alzaatreh, C. Lee, F. Famoye, A New Method for Generating Families of Continuous Distributions, Metron 71 (2013), 63–79. https://doi.org/10.1007/s40300-013-0007-y.

[4] WHO, WHO Recommendations for the Prevention and Treatment of Postpartum Haemorrhage, World Health Organization, 2012.

[5] L. Say, D. Chou, A. Gemmill, Ö. Tunçalp, A.B. Moller, et al., Global Causes of Maternal Death: A WHO Systematic Analysis, Lancet Glob. Health 2 (2014), e323–e333. https://doi.org/10.1016/S2214-109X(14)70227-X.

[6] Wikipedia, Health in Nigeria, Wikipedia, 2023, (Accessed 15 August 2025). https://en.wikipedia.org/wiki/Health_in_Nigeria.

[7] J. Tukur, T. Jido, B. Awolaja, Maternal Mortality in Rural Northern Nigeria, Trop. Dr. 38 (2008), 35–36. https://doi.org/10.1258/td.2006.006356.

[8] A. Patel, S. Goudar, S. Geller, B. Kodkany, S. Edlavitch, et al., Drape Estimation Vs. Visual Assessment for Estimating Postpartum Hemorrhage, Int. J. Gynecol. Obstet. 93 (2006), 220–224. https://doi.org/10.1016/j.ijgo.2006.02.014.

[9] P. Toledo, R.J. McCarthy, B.J. Hewlett, P.C. Fitzgerald, C.A. Wong, The Accuracy of Blood Loss Estimation After Simulated Vaginal Delivery, Anesth. Analg. 105 (2007), 1736–1740. https://doi.org/10.1213/01.ane.0000286233.48111.d8.

[10] H.M. Aljohani, The New Explanation of Lomax Distribution: Its Properties, Inference, and Applications to Real-Life Data, Contemp. Math. (2025), 2541–2569. https://doi.org/10.37256/cm.6220255778.

[11] J.Y. Falgore, A.A. Umar, A. Yakubu, A.I. Ishaq, The Inverse Lomax Distribution with Applications, in: Royal Statistical Society Nigeria Local Group 2025 Conference Proceedings, pp. 105–112, 2025.

[12] B. Madsen, H. Lilholt, L.P. Mikkelsen, R. Kumar, Datasets From Tensile Testing of Unidirectional Carbon Fibre Composites Using Different Specimen Types, Zenodo, 2021. https://doi.org/10.5281/zenodo.5092028.

[13] C.C. Ishiekwene, B.A. Afere, Higher-Order Hybrid Gaussian Kernel in Meshsize Boosting Algorithm. AFR-REV STECH 1 (2014), 81–91.

[14] Z. Birnbaum, S. Saunders, A New Family of Life Distributions, J. Appl. Probab. 6 (1969), 319–327. https://doi.org/10.2307/3212003.

[15] I. ALI, Cosine Kumaraswamy Family of Distributions: Properties and Applications to Real-World Datasets, Sigma J. Eng. Nat. Sci. 43 (2025), 2186–2197. https://doi.org/10.14744/sigma.2025.1935.

[16] University College Hospital, Ibadan, University College Hospital, Ibadan, 2023. (Accessed 19 August 2025). https://uch-ibadan.org.ng.

[17] S. Nadarajah, S. Kotz, The Beta Exponential Distribution, Reliab. Eng. Syst. Saf. 91 (2006), 689–697. https://doi.org/10.1016/j.ress.2005.05.008.

[18] S.O. Bashiru, A.M. Isa, A.A. Khalaf, M.A. Khaleel, et al. A Hybrid Cosine Inverse Lomax-G Family of Distributions with Applications in Medical and Engineering Data, Niger. J. Technol. Dev. 22 (2025), 261–278. http://dx.doi.org/10.4314/njtd.v22i1.2734.

[19] F. Famoye, C. Lee, O. Olumolade, The Beta-Weibull Distribution, J. Stat. Theory Appl. 4 (2005), 121–136.
[20] S.O. Bashiru, A.A. Khalaf, A.M. Isa, A. Kaigama, On Modeling of Biomedical Data With Exponentiated Gompertz Inverse Rayleigh Distribution, Reliab. Theory Appl. 19 (2024), 460–475.
[21] R.D. Gupta, D. Kundu, Theory & Methods: Generalized Exponential Distributions, Aust. New Zealand J. Stat. 41 (1999), 173–188. https://doi.org/10.1111/1467-842x.00072.
[22] S.O. Bashiru, I.I. Itopa, A.M. Isa, On the Properties of Generalized Rayleigh Distribution With Applications, Reliab. Theory Appl. 3 (2023), 374–386. https://doi.org/10.24412/1932-2321-2023-374-374-386.
[23] W. Barreto-Souza, A.H.S. Santos, G.M. Cordeiro, The Beta Generalized Exponential Distribution, arXiv:0809.1889, 2008. https://doi.org/10.48550/arXiv.0809.1889.
[24] R. Alshkaki, A Generalized Modification of the Kumaraswamy Distribution for Modeling and Analyzing Real-Life Data, Stat. Optim. Inf. Comput. 8 (2020), 521–548. https://doi.org/10.19139/soic-2310-5070-869.
[25] A.L. Bowley, Elements of Statistics, 6th ed., Staples Press Limited, 1920.
[26] J.J.A. Moors, A Quantile Alternative for Kurtosis, Statistician 37 (1988), 25–32. https://doi.org/10.2307/2348376.
[27] C.E. Shannon, A Mathematical Theory of Communication, Bell Syst. Tech. J. 27 (1948), 379–423. https://doi.org/10.1002/j.1538-7305.1948.tb01338.x.
[28] E. LIMPERT, W.A. STAHEL, M. ABBT, Log-Normal Distributions Across the Sciences: Keys and Clues, BioScience 51 (2001), 341–352. https://doi.org/10.1641/0006-3568(2001)051[0341:lndats]2.0.co;2.
[29] K.S. Lomax, Business Failures: Another Example of the Analysis of Failure Data, J. Am. Stat. Assoc. 49 (1954), 847–852. https://doi.org/10.1080/01621459.1954.10501239.
[30] P. Kumaraswamy, A Generalized Probability Density Function for Double-Bounded Random Processes, J. Hydrol. 46 (1980), 79–88. https://doi.org/10.1016/0022-1694(80)90036-0.
[31] G.M. Cordeiro, M. de Castro, A New Family of Generalized Distributions, J. Stat. Comput. Simul. 81 (2011), 883–898. https://doi.org/10.1080/00949650903530745.
[32] B.A.E. Afere, Hybrid-Epanechnikov Transformed Kumaraswamy Distribution: Applications to COVID-19 Mortality and Survival Analysis, Fac. Nat. Appl. Sci. J. Appl. Biol. Sci. 2 (2024), 49–63.